Microtubule-mediated nuclear deformation drives the Epithelial-to-Mesenchymal Transition and breast cancer.

Mar Arias Garcia[1], Rebecca Rickman[1], Julia Sero[1], Yinyin Yuan [2,3], Chris Bakal [1,2,3]

[1] Dynamical Cell Systems Team. Chester Beatty Laboratories, The Institute of Cancer Research, 237 Fulham Road, London UK, SW3 6JB

[2] Computational Pathology and Integrative Genomics Team. The Institute of Cancer Research, 15 Cotswold Road, Sutton, SM2 5NG

[3] Address correspondence to **yinyin.yuan@icr.ac.uk** and **chris.bakal@icr.ac.uk**

Short title: Microtubule-mediated nuclear deformation promotes EMT

Abstract

The Epithelial-to-Mesenchymal transition (EMT) is a cell state change essential for the development and homeostasis of all metazoan organisms. EMT-like programmes also drive metastasis in tumour cells. Classical studies have demonstrated that mechanical and geometric cues, such as the disruption of cell-cell adhesion can induce EMT. But how these cues are converted into cell fate decisions through changes in transcriptional activity are not well understood. Using an image-omic approach we identify Junctional Adhesion Molecule 3 (JAM3) as a tumour suppressor in breast cancer patients, and a suppressor of EMT in breast epithelial cells. Engagement of EMT following JAM3 depletion is due to changes in nuclear shape caused by microtubules, and resulting activation of pro-EMT factors such as YAP and TAZ. Critically, uncoupling microtubules from the nucleus reverts EMT. These results provide a mechanistic basis for the long-standing observations of how loss of cell-cell adhesion leads to EMT and cancer.

Introduction

The ability of epithelial cells to change into mesenchymal forms is essential for the development of tissues and homeostatic processes such as gastrulation, neural crest migration, and wound healing[1]. The change in shape, from an apicobasally polarized epithelial cuboidal cell with cell-cell adhesions, to a protrusive mesenchymal cell with leading edge/trailing edge polarity and extensive cell-extracellular matrix (ECM) adhesions, is driven by extensive transcriptional changes[2]. Engagement of EMT-like programmes, such as "hybrid" or "partial" EMT [3] by cancer cells also promotes the acquisition of stem cell traits, elevated drug resistance, and drives metastasis[4, 5]. Both full and partial EMT can be triggered by biophysical cues, such as loss of cell-cell adhesion, increased matrix elasticity, and changes in ECM geometry[6-9]. For example, classic work by Greenburg and Hay demonstrated that a change in the mechanical and geometric properties of the environment alone, in particular suspending epithelia in 3D matrices, is sufficient to trigger EMT[10]. But how the fluctuation of mechanical and geometric cues in a tissue can change cell state, and potentially drive diseases such as cancer, is very poorly understood.

One means by which mechanical cues affect the engagement of transcriptional programmes is through changes in nuclear shape and stiffness[11-16]. Although nuclei are often considered to be largely oval/spherical, different nuclear shapes are associated with different cell states. For example, nuclei undergo extensive shape changes during differentiation[17]. Nuclear shape affects transcription in part by affecting the nuclear translocation of transcription factors such as YAP/TAZ and NF-κB[18, 19]. Thus mechanical cues and changes in cell geometry can affect nuclear shape, which in turn regulates cell fate by altering transcription factor dynamics. But how nuclear changes are regulated by environmental fluctuations is virtually unknown.

Conversely, mechanisms exist to maintain nuclear shape, or nuclear "morpheostasis", when cells are exposed to external forces such as stretch, strain, and compression. Disruption of nuclear shape is coincident with numerous diseases including cancers, heart disease, and aging disorders such as progeria[20]. In epithelial cells, the anchoring of microtubule (MT) minus-ends at cell-cell adhesion complexes results in the stabilization, nucleation, and polymerization of MTs along the apicobasal axis[21-25]. The orientation of MTs in epithelial cells results in the capture of plus-end MTs by nuclear bound SYNE-4, a Nesprin that is part of SUN-KASH complexes that interact with plus-end directed Kinesin-1 motors[11]. MTs which

bridge cell-cell adhesions and the nucleus can act to cushion the nucleus from any deformation that can occur when epithelial tissues are exposed to external forces [26].

The importance of maintaining nuclear shape to cell, tissue, and organism homeostasis is highlighted by the fact that changes in nuclear morphology are particularly associated with cancer. Indeed, pathologists have used nuclear shape as a diagnostic for decades[27]. Irregular nuclear shapes and sizes, or pleomorphisms, are often hallmarks of cancer cells; whereas smooth, roundish forms are characteristic of normal cells[28]. Both the cause and consequences of these nuclear shape deformations to oncogenesis are not clear. In some cancer cells a highly deformable nucleus is necessary to squeeze through small pores (<10 microns) in 3D environments during confined migration[29]. Dysregulation in nuclear morphogenesis is also linked to genome instability[30], alterations in the dynamics of DNA damage repair pathways[31, 32], and activation of pro-inflammatory pathways [33] – all of which can contribute to tumorigenesis and metastasis.

How forces are absorbed by the cytoskeleton to promote nuclear morpheostasis, or propagated to the nucleus resulting in deformation during cell fate decisions such as differentiation is unclear. We reasoned that dysregulation of the force absorbing/propagating mechanism in epithelial cells may be a primary mechanism of breast cancer oncogenesis. Thus, we used an image-omic approach to identify genes associated with nuclear shape changes in breast cancer patients. Our analysis revealed that the gene encoding the cell-cell adhesion component JAM3 is a tumour suppressor that maintains nuclear shape *in vivo*. We show that in normal breast epithelial cells JAM3 suppresses EMT, prevents invasion, and inhibits YAP/TAZ activation by maintaining MTs in an epithelial-type configuration. Depletion of JAM3 results in MT reorganization, from an epithelial to a mesenchymal type configuration that affects nuclear shape and nuclear lamin architecture, driving pro-EMT transcriptional programmes. EMT following JAM3 depletion can be reversed by uncoupling MTs from the nucleus, inhibiting TAZ translocation, or chemically blocking Kinesin-1 binding to MTs. We show that JAM3 depletion-induced EMT in 3D cultures following is dependent on TAZ but not YAP. These data provide a mechanistic basis for the long-standing observations that disruption of cell-cell adhesion can cause differentiation of epithelial cells into mesenchymal states, and how dysregulation of pathways that maintain nuclear morpheostasis during fluctuations in biophysical forces can drive breast cancer tumorigenesis and metastasis.

Results

Hybrid network topological analysis revealed tumour morphology-driven gene expression

To understand how changes in nuclear shape may drive tumorigenesis, and to identify genes that might be important for nuclear shape homeostasis, we identified genes whose levels correlated with changes in nuclear shape in 1,000 invasive human breast tumours. We described the shape of single cancer cell nuclei and the morphological heterogeneity of tumour cell nuclei *in vivo* by quantifying six shape features of tumour cell nuclei, but not the nuclei of lymphocytes or stromal cells, in haematoxylin and eosin (H&E) stained sections (Supplemental Table 1; Figure 1A). For all features, a higher value indicates more irregular/elongated morphology, whilst a low value indicates a regular/round morphology. On average, there were 6×10^4 cancer cells in the H&E sections in each tumour, and we used three statistics – median, standard deviation (sd), and skewness – to characterize the distribution of nuclear shape features in a tumour (Figure 1A). In total, 18 nuclear morphology scores were obtained for each tumour. Batch effects arising from different hospital sites and different staining and processing procedures were corrected for (Methods).

To identify cancer-driven molecular changes, we first identified the top 1,000 cis-driven genes based on association between DNA copy number alterations and mRNA expression across the 1,000 invasive breast cancers. This method was used previously for the discovery of 10 breast cancer subtypes[34]. We then determined how the expression and copy number of these genes correlated with nuclear morphology and cell-to-cell nuclear shape variability. The strongest gene expression-nuclear shape associations were used to construct a hybrid network ($q<0.01$ of false discovery rate (FDR) corrected Spearman correlation), with the core network module connecting 6 morphological scores and 38 gene expression probes representing 32 unique genes ($q<0.005$, Figure 1B). Nodes represent morphological scores or genes and edges denote significant correlations. Given that these genes were pre-selected based on their copy-number and gene expression profiles, this network effectively links DNA copy number, gene expression, and nuclear morphology.

Topology analysis of this network revealed that a morphological score “median I1” was positioned as the best-connected network hub (Methods). This feature describes rotational stability given the shape of an object. Intuitively, an object with irregular shape has a high I1 value. Cells and tumour tissues with different median I1 values are shown in Figures 1C and 1D. We henceforth refer to this morphological score as the Cancer Nuclear Instability index (CNI). Notably, “instability” here refers to a morphological property, as opposed to genomic

instability. Well-differentiated epithelial-like cells have high CNI, whereas low CNI cells have abnormally-shaped nuclei (Figure 1D). Consistent with the idea that low CNI is a marker of cancer progression and aggressiveness, this score was strongly and negatively associated with the mRNA levels of genes previously implicated in breast tumorigenesis including MCM4[35], MCM10[36], FOXM1[37], CCNE2[38], and MASTL[39] (Figure 1B). In addition, besides median I1 as an average measure, heterogeneity measures including standard deviation and skewness of morphology scores were also identified in this core network module; indicating that gene expression in single cells correlates with the exent of nuclear morphology heterogeneity in the population. Thus both median changes in nuclear morphology, as well as cell-to-cell variability in nuclear morphology are coupled to transcriptional upregulation of known oncogenes.

JAM3 depletion correlates with heterogeneity in nuclear morphology

To identify genes that are positively associated with CNI, and thus are putative tumour suppressors, we performed correlation analysis of CNI and genome-wide gene expression revealing 735 significant correlations (FDR correction q<0.01). CNI positively correlated with the mRNA expression of a number of genes encoding components of cell-cell adhesions, among which is JAM3 (Junctional Adhesion Molecule 3) whose mRNA was highly correlated with CNI (correlation=0.37, q-value 2.9×10^{-6}) (Figure 2A). JAM3 mRNA expression was strongly cis-driven (FDR corrected Spearman correlation among genome-wide associations between copy number and expression q-value=1×10^{-7}) and was predominately lost in breast cancer (13% copy-number loss and only 0.8% gains; Figure 2B). The expression of JAM3 mRNA was lower in Basal, HER2, and Luminal B subtypes compared to the Luminal A subtype and “normal” subtypes (Figure 2C). JAM3 mRNA expression differed significantly in the 10 subtypes, among which “IntClust4” and “IntClust10” subtypes had the highest and lowest levels of JAM3 mRNA respectively (Figure 2D). IntClust4, which had high JAM3 mRNA expression, is the ‘CNA-devoid’ (no copy number alteration) group with favourable prognosis and a significant proportion of cases presented with extensive lymphocytic infiltration[34]. IntClust10, which has low JAM3 mRNA expression, includes the majority of Basal-like samples with high genomic instability. JAM3 mRNA expression was also upregulated in invasive lobular carcinoma (ILC) compared with the more aggressive invasive ductal carcinoma (IDC) histology type (Figure 2F). The expression of JAM3 mRNA also negatively correlated with tumour grade (Figure 2F). We therefore predicted that *JAM3* is a breast tumour suppressor gene. Because JAM3 loss correlates with changes in nuclear shape, we further predicted that JAM3 deficiency drives oncogenesis by changing nuclear shape.

JAM3 regulates microtubule and nuclear morphogenesis

To investigate the role of JAM3 in regulating nuclear shape, we used quantitative single cell morphological analysis[40] to asses how depletion of JAM3 affected the cell and nuclear shape of non-transformed MCF10A mammary epithelial cells. To this end, we used single or pooled small interfering RNAs (siRNAs) that effectively reduced JAM3 mRNA and/or protein. We observed two different pools (siGENOME or "siG", and On-Target Plus or "OTP") reduced JAM3 mRNA levels by 95 percent, and all individual siRNAs that made up each pool reduced JAM3 mRNA levels between 75 and 97 percent (Figure S1A). Consistent with previous reports[41-44], JAM3 protein is localized to the cell-cell junctions of MCF10A non-transformed epithelial cells, and the siG pool reduced JAM3 to virtually undetectable levels as judged by immunofluorescence (Figure 3A). The siG and OTP pools effectively depleted JAM3 protein in MCF10A as judged by Western blotting (Figure S1B). Although both siRNA pools and all individual siRNAs are highly effective at reducing JAM3 mRNA, for the majority of our experiments we used the siG pool and/or a single siRNA, OTP5, to deplete JAM3.

Depletion of JAM3 by different siRNAs did not disrupt the ability of MCF10As to form cell-cell adhesions, as shown by the overall morphology of highly confluent cultures, and the accumulation of β-catenin at cell-cell borders. However, the β-catenin positive cell-cell junctions in JAM3 knockdown cells had altered morphology compared to mock treated junctions and appeared "jagged" (Figure 3A). But in contrast to the relatively mild effects on cell-cell adhesion, depletion of JAM3 by siRNA resulted in the dramatic reorganization of MT structures. Whereas the MTs of wild-type cells were organized into parallel filaments that span the long axis of the cell, and loosely grouped in the perinuclear region (Figure 3B arrows); the MTs of JAM3 depleted cells were consistently organized into radial arrays with highly focused microtubule organizing centres (MTOC) (Figure 3B chevrons). Differences in MT organization between wild-type and JAM3 depleted cells were quantified by measuring the intensity of MTs in the perinuclear region (Figure 3C). These data suggest that JAM3 is not essential for the formation of cell-cell adhesions, but does contribute to adhesion organization, and regulates MT morphogenesis.

JAM3 depletion in MCF10A cells also resulted in striking changes in nuclear morphology. The vast majority of nuclei of normal MCF10A cells were shaped like smooth ovals. In contrast, the nuclei of JAM3 depleted cells had a highly irregular, "banana" shapes, and a proportion of even had large holes in the nuclei (Figure 3B asterisks). We termed the nuclei with large holes "donuts". Using a linear classifier we automatically identified donut nuclei in cellular populations (Methods). Normal cell populations had ~1% of nuclei that could be classified as donuts, but JAM3 depletion increased the proportion of donut nuclei population

to ~10-20% (Figure 3D). Inhibition of JAM3 by 3/4 individual siRNAs from the siG pool (Figure S1C), or 2/4 siRNAs from the OTP pool (Figure S1D) led to significant increases in donuts, eliminating the possibility this phenotype can be attributed to off-target effects. The MTOC of JAM3 depleted cells was almost always positioned in the hole of nuclear donuts, or at deepest point of invagination in banana nuclei (Figure 3C, arrow). Knockdown of JAM3 in other normal epithelial cell types, such as Retinal Pigmented Epithelial (RPE-1) cells also had similar effects (Figures S1D and S1E). Taken together, these data suggest that JAM3 plays an important role in normal epithelial cell and nuclear morphogenesis.

JAM3 suppresses EMT and cell invasion

Based on the change in MT organization following JAM3 depletion, from thin parallel filaments reminiscent of non-centrosomal MT arrays in epithelial cells, to bundled radial arrays characteristic of mesenchymal cells[24] following JAM3 depletion, we hypothesized that JAM3 suppresses EMT[2]. To test this idea, we asked whether JAM3 depletion resulted in MCF10A cells gaining the ability to invade 3D collagen matrices. Whereas normal MCF10A do not invade collagen matrices, JAM3 depleted cells invaded the gels to depths of 60 μms in 24 hrs (Figure 3E). Collagen invasion was dependent on Matrix Metalloproteinases (MMPs; Figure 3F). The EMT phenotype following JAM3 loss was confirmed by the observation that JAM3 deficient cells upregulate pro-mesenchymal mRNAs including Fibronectin-1 (FN), ITGA5, MMP3, BMP1, and MAP1B, and downregulate pro-epithelial mRNAs such as KRT14 and KRT19 (Figure 3G). We confirmed upregulation of an EMT program through qPCR of individual mRNAs (Figure S1F). Thus JAM3 is required for transcriptional suppression of EMT programmes.

To explore whether changes in nuclear and MT morphology occur during EMT induced by other stimuli, we treated MCF10A cells for 48 hrs with TGF-β. EMT caused by TGF-β coincided with significantly increases in the sub-population of cells with low nuclear roundness to a similar extent as JAM3 depletion alone. Addition of TGF-β to JAM3 depleted cells nearly doubled the population of cells with low nuclear roundness (Supplemental Figure S2A). We also quantified the distribution of the plus-end binding protein EB1, from which the organization of the MT arrays can be inferred, following JAM3 depletion +/- TGF-β stimulation. In MCF10A cells in an epithelial-like state, EB1 was predominantly distributed as small parallel filaments in the cytoplasm. In JAM3 depleted cells, in TGF-β treated cells, or in TGF-β treated JAM3 depleted cells, EB1 was primarily localized to the cell periphery and the leading edge (Supplemental Figure S2B, S2C). Taken together these data support the idea that nuclear deformation and changes in MT organization commonly occur during EMT.

JAM3 is required for the morphogenesis of epithelial tissues

To asses the role of JAM3 in promoting epithelial morphogenesis, we investigated the ability of JAM3-deficient MCF10A cells to form 3D acini structures in solid matrices in mixtures of Matrigel and collagen-I (Col-I)(Methods). Following two days in 3D matrices normal MCF10A cells formed round structures with a well-organized thin outer basement membrane layer, as shown by laminin-5 staining (Figure 4A,B). In contrast, JAM3 depletion decreased both the total number of acini and the number cells in each acinar structure (Figure 4A,B). JAM3-depleted acini also frequently formed large F-actin rich protrusions (Figure 4A, arrows) and extensively remodelled both laminin-5 and FN matrix (Figure 4A, chevrons). The laminin-5 basement membrane in JAM3-depleted acini was virtually non-existent compared to wild-type, but FN was organised into large bundles that encapsulated the acini (Figure 4A, chevrons). Over eight days, JAM3-depleted acini developed into irregularly shaped, invasive structures, and JAM3-depleted, but not wild-type, acini migrated towards each other (Supplemental Movie S1 and S2), and often fused into larger multi-acinar structures (Figure 4C, 4D). These results demonstrate JAM3 is essential for mammary acini morphogenesis in 3D, and suggest that JAM3 suppresses EMT.

JAM3 suppresses the activity of YAP and TAZ

We hypothesized that because JAM3 depletion alters microtubule and nuclear morphogenesis, which coincides with EMT, this may result in nuclear translocation and activation of the YAP and/or TAZ transcriptional co-activators. Both YAP and TAZ translocate from the cytoplasm to nucleus in response to forces on the nucleus[19, 45], and regulate the transcription of genes that promote EMT[46-48]. In wild-type MCF10A cells cultured at medium to high densities, both YAP and TAZ are predominantly localized to the cytoplasm as determined by immunofluorescence staining (Figure 5A,B) using antibodies specific to these proteins (Figure S4A, S4B, S4C). However, both YAP and TAZ localize to the nucleus after downregulation of JAM3 as determined by immunofluorescence (Figure 5A,B). To confirm that JAM3 depletion results in a change in the subcellular localization of YAP and TAZ, we performed biochemical fractionation of mock-treated and JAM3 depleted cells, and quantified the levels of YAP and TAZ in each fraction by Western blotting. Indeed, JAM3 depletion resulted in a significant accumulation of both YAP and TAZ in the nucleus (Figure 5C), and depletion of YAP and TAZ from membrane fractions (Figure 5D). Finally, we observed that CTGF mRNA is also upregulated following JAM3 depletion (Figure 5E). Taken together, these data suggest JAM3 is required to suppress the activity of YAP and TAZ in epithelial cells.

We next determined YAP and/or TAZ are required for the mesenchymal phenotypes of JAM3-depleted cells. Whereas JAM3 depletion increased the production of extracellular Col-I, co-depletion of JAM3 with YAP and TAZ or YAP alone its production (Figure S5A). Similarly, co-depletion of JAM3 with YAP and TAZ, or with TAZ alone suppressed the production of extracellular FN protein (Figure S5B). Thus, JAM3 depletion results in remodelling of the ECM through YAP-dependent production of Col-I, and TAZ-dependent production of FN. To asses whether YAP or TAZ are required for EMT in 3D acini, we knocked down YAP or TAZ in JAM3-deficient MCF10A organoids. YAP or TAZ depletion did not prevent the formation of acini (either normal or abnormal) following JAM3 depletion over two days (Figure 6A) Both JAM3 depletion alone and co-depletion of JAM3 and YAP1 resulted in acini with multiple actin-rich protrusive structures (Figure 6A, 6B). However, depletion of TAZ completed abrogated the formation of actin-rich invasive structures in the absence of JAM3 (Figure 6A, 6B). Thus, engagement of an EMT programme induced by loss of JAM3 is dependent on TAZ.

Uncoupling the nucleus from the MT cytoskeleton rescues the JAM3 depletion nuclear phenotype and induction of EMT

Given the abnormally close proximity of the MTOC to the nucleus of JAM3 depleted cells, we reasoned that changes in nuclear morphology may be due to abnormal physical forces placed upon the nucleus by the MTs. In epithelial cells, both the actin and MTs cytoskeletons are directly coupled to the nucleus via SUN-KASH complexes[11]. SUN1 and SUN2 are ubiquitous members of these complexes that are embedded into the nuclear membrane, and Nesprin/SYNE proteins serve as adaptors which link SUN1/2 to specific cytoskeletal components. The kinesin-1 heavy chain KIF5B interacts with SYNE4 to couple MTs to the nucleus [49]. We systematically depleted all known SUN-KASH components individually, as well as SYNE4 and KIF5B in combination, in JAM3-depleted cells to determine if uncoupling the nucleus from the cytoskeleton rescued nuclear and MT phenotypes. Only co-depletion of JAM3, SYNE4, and KIF5B (hereafter referred to as the “triple” knockdown) led to a complete reversion of the abnormal nuclear shape (Figure 7A) and MT phenotypes (Figure 7B) observed in JAM3 deficient cells alone. Donut nuclei and a dense MTOC were clearly observed in all conditions except the triple knockdown (Figure 7C, chevrons). These results support the idea that loss of JAM3 results in a change in MT organization that causes alterations in nuclear morphogenesis, and that uncoupling the physical links between the MTS and the nuclear membrane relieves JAM3-depleted nuclei of forces placed upon them by the MT cytoskeleton. Moreover, these data suggest that kinesin motor activity promotes nuclear morpheostasis in epithelial cells, and is critical in deforming nuclear shape when cell-cell adhesion is disrupted.

To determine if restoring nuclear morphogenesis by uncoupling the nucleus from the MTs also prevented EMT, we measured 3D invasion, CTGF expression, and YAP or TAZ nuclear translocation in: 1) normal cells; 2) cells depleted of JAM3, KIF5B, or SYNE-4 alone; 3) cells co-depleted of JAM3 and KIF5B or SYNE-4; and 4) cells co-depleted of JAM3, KIF5B, and SYNE-4 (triple knockdown). Whereas depletion of JAM3 alone, or co-depletion of JAM3 and KIF5B or SYNE-4, led to increased invasion, the triple knockdown cells did not invade (Figure 7D). Depletion of both SYNE-4 and KIF5B in combination with JAM3 also reduced CTGF mRNA expression (Figure 7E), nuclear YAP (Figure 7F) and nuclear TAZ (Figure 7G) compared to JAM3 knockdown alone. The ability of triple RNAi to restore YAP and TAZ nuclear levels to those of wild-type was confirmed by Western blotting for YAP and TAZ in lysates following subcellular fractionation (Figure 7I,J). Thus, the function of both KIF5B and SYNE-4 are required for EMT following depletion of JAM3. These data support the idea that loss of JAM3 results in cytoskeletal changes that cause nuclear deformation, YAP/TAZ activation, and EMT; and that uncoupling the nucleus from the MTs prevents EMT induced by nuclear deformation

Loss of JAM3 disrupts the organization of the nuclear lamina

The defects in nuclear morphogenesis following JAM3 depletion were highly reminiscent of nuclear morphology defects observed in cells with dysfunctional Lamin A (LMNA), such as progeric cells (Eriksson et al., 2003). The viscoelastic properties of the nucleus are partly determined by the levels of both LMNA and LMNB, although LMNA levels have been observed to vary to much greater extents that LMNB, suggesting that the LMNA:LMNB ratio is a key factor in determining nuclear viscoelasticity[50, 51]. In support of this idea, depletion of LMNA, but not LMNAB, increased the percentage of misshapen nuclei in the population, and that of donuts in particular (Figure 8A). But while combined depletion of LMNA and JAM3 also led to a marked increase in the percentage of misshapen nuclei in the population, the nuclei of JAM3 and LMNB deficient cells were the same shape as wild-type nuclei (Figure 8B chevrons). Because reduction of LMNB, but not LMNA, restores the nuclear morphology defects in JAM3 cells, we propose the effects on JAM3 depletion are at least in part due to decreased level of LMNA relative to LMNB, and thus the viscoelasticity of the nucleus.

We next sought to determine whether JAM3 regulates LMNA and/or LMNB levels or localization in a manner that is dependent on SYNE4 and KIF5B. Antibodies specific to LMNA and LMNB (Figure S6A, S6B) were used to detect either the total levels of nuclear LMNA and LMNB (Figure 8C). The ratio of LMNA or LMNB localized to the nuclear ring region compared to the inner ring region was measured as a proxy for the amount of each

protein that is incorporated into the nuclear lamina (Figure 8D, 8E, Figure S5B). Depletion of JAM3 affected both the outer:inner nuclear ratio of LMNA (Figure 8C, 8D) and LMNB (Figure 8C, 8E). Combined depletion of SYNE4 and KIF5B in the background of JAM3 depletion (the "triple" knockdown) restored the levels of LMNA (Figure 8D) but not LMNB (Figure 8E) in the nuclear lamina. The alterations in LMNA and LMNB localization following JAM3 depletion were not due to decreases in either LMNA or LMNB mRNA levels (Figure S6C), or the ratio of LMNA:LMNB mRNA (Figure S6D). However, JAM3 depletion did decrease the total levels of nuclear LMNA (Figure S6E), but not LMNB (Figure S6F), and the total intensity of LMNB in the lamina (Figure 5F). The amount of LMNA in the nuclear lamina (Figure 8D, F) and total LMNA levels (Figure S6E) were rescued by the triple knockdown. However, LMNB outer:inner nuclear ratio levels (Figure 8E) and total LMNB levels (Figure S6F) were similar in the JAM3-depleted and control cells. In fact, LMNB intensity in the outer nucleus was elevated in triple knockdown cells compared to control (Figure 8F). These data support the idea that JAM3 depletion and MT reorganization affect nuclear viscoelasticity by reducing LMNA levels and altering the LMNA:B ratio – leading to a "softer" nucleus.

Because phosphorylation of LMNA at serine 22 (hereafter referred to a pLMNA) promotes the dissociation of LMNA filaments[52, 53], we measured Ser22 phosphorylation following JAM3, SYNE4 and/or KIF5B. Depletion of JAM3 significantly increased the total levels of pLMNA (Figure 8G). Increased pLMNA levels were completely rescued in the triple knockdown. In summary, these data suggest that JAM3 regulates the incorporation of LMNA into the nuclear lamina as well as LMNA stability.

JAM3 suppresses YAP/TAZ activation and EMT via nuclear mechanics

Interestingly, knocking down both YAP and TAZ rescued the decrease of LMNA in the nuclear matrix caused by JAM3 depletion (Figure 8D, S6E), but did not affect LMNB (Figure 8E, S6F). Conversely, co-depletion of LMNB, but not LMNA, with JAM3 restored levels of active YAP/TAZ to that of control cells (Figure S6G, S6H). However, of the total amounts of both LMNA and LMBA were markedly increased in JAM3/YAP/TAZ knockdown nuclei compared to controls. Taken together these data suggest that following loss of JAM3, physical forces on the nucleus mediated by the MTs promote YAP/TAZ activation, which in turn leads to reduced LMNA protein. Decreases in LMNA alter the viscoelasticity of the nucleus, which then results in further deformation of the nucleus by the MTs. But the translocation of YAP/TAZ itself is also likely dependent on the viscoelasticity of the nucleus, as co-depletion of JAM3 and LMNB, also inhibits YAP/TAZ translocation. We propose that pro-EMT programmes mediated by YAP/TAZ act to decrease nuclear viscoelasticity in both

transcriptional and post-transcriptional (mechanical) fashions – establishing feed-forward loops.

To determine if changes in nuclear viscoelasticity underpinned the ability of JAM3-depleted cells to invade collagen gels, we monitored invasion in JAM3 cells co-depleted of LMNA or LMNB. Loss of LMNA alone promoted invasion and synergistically enhanced JAM3 knockdown cell invasion (Figure S6I). However, depletion of LMNB did not promote invasion or alter the ability of JAM3-depleted cells to invade (Figure S6I). Thus we conclude that decreases in LMNA protein levels, increases in pLMNA phosphorylation, dissociation of LMNA filaments, and decreases in nuclear stiffness facilitate invasion following loss of JAM3.

To gain further insight into the role of Kinesin-1 function in maintaining nuclear shape in normal epithelial cells, and distorting nuclear shape in JAM3 depleting cells, we treated JAM3, or JAM3/SYNE4 deficient cells, with Rose Bengal Lactone (RBL) a fluorescein compound that binds Kinesin-1 at the L8/β5 pocket and inhibits the binding of Kinesin-1 to MTs[54]. RBL rescued nuclear morphology defects in both JAM3 and JAM3/SYNE4 depleted cells (Figure S7A, S7C), and the levels of LMNA in the outer matrix (Figure S7B, S7C). Thus we propose in epithelial cells Kinesin-1 binding to MTs promotes nuclear morpheostasis, but in JAM3 depleted mesenchymal-like cells Kinesin-1 promotes nuclear deformation.

JAM3 does not regulate the cell cycle or protect against DNA damage

To determine whether the JAM3-KIF5B-SYNE4-YAP/TAZ axis affects cell cycle progression, we quantified the percentage of G1, S, and G2 cells in cells depleted of: JAM3 alone; JAM3 in combination with KIF5B and/or SYNE4; or JAM3 in combination with YAP and TAZ (Figure S8A). We confirmed these observations by quantifying the number of mitotic cells (Methods; Figure S8B). JAM3 depletion had only a mild effect on proliferation, with fewer cells in S/G2 but comparable numbers of mitotic cells to control populations. Knocking down either YAP or TAZ alone produced partial G1 arrest, as depletion of both proteins is required to completely inhibit proliferation (Figure S8B), and co-depletion of JAM3 did not exacerbate or rescue these phenotypes. Spindle assembly appeared unaffected in JAM3 depleted cells (Figure S8C). Interestingly, both KIF5B and SYNE4 depletion alone had much more profound effects on cell cycle progression than JAM3 depletion, but these phenotypes were rescued by co-depletion with JAM3. (Figure S8A, S8B). We that uncoupling epithelial MTs from the nucleus, but not cell-cell adhesion complexes, disrupts nuclear morpheostasis and cell cycle progression. But that disrupting MT attachments to cell-cell adhesions, and

reorganizing the MTs into a radial array, can prevents any defects in cell cycle progression associated with loss of nuclear-MT attachments.

To determine if nuclear morphogenesis defects resulted in an increased in damaged DNA, we quantified the levels of gammaH2AX in wild-type cells or JAM3 knockdown cells depleted of KIF5B, SYNE4, KIF5B + SYNE4, YAP, YAP + TAZ, TP53 (as positive control of increased DNA damage). Only knockdown of TP53, SYNE4 or TAZ resulted in increased numbers of gammaH2AX levels (Figure S8D, S8E). Interestingly, while knockdown of JAM3 rescued the increased DNA damage observed in SYNE4 and TP53 depleted cells, it did not affect gammaH2Ax levels in the absence of TAZ. Taken together, these data suggest that nuclear morphogenesis defects in JAM3 depleted cells do not increase DNA damage, and in fact changes in nuclear viscoelasticity following JAM3 depletion may even prevent DNA damage driven by TP53 or SYNE4 depletion.

JAM3 expression is associated with good prognosis

To validate JAM3's role as a tumour suppressor in patients, we performed survival analysis using JAM3 expression and disease-specific survival in different subgroups of breast cancer. We observed that in all subgroups with elevated levels of JAM3 (Luminal A, ILC, and Normal-like intrinsic subtypes), JAM3 expression is correlated with favourable prognosis (Figure 9A). Increased JAM3 expression also predicts relapse-free survival after treatment in patients with Luminal A type tumours (Figure 9B). Thus JAM3 is a *bona fide* tumour suppressor in breast cancer patients.

Given the induction of EMT, and concomitant increased invasiveness of JAM3 depleted MCF10A cells, we next sought to determine if JAM3 altered the metastatic potential of breast tumour cells in patients. Although all forms of metastasis may not depend on classical EMT [55-57], the metastasis of cells to stiff tissues such as bone likely requires matrix remodelling proteins such as MMPs whose levels are elevated during EMT[58, 59]. Indeed, we observed a 1.6-fold increase of bone metastasis in cases with JAM3 loss compared with copy number neutral cases (Figure 9C), which suggests that JAM3 suppresses EMT and metastasis *in vivo*.

We reasoned that if JAM3 promotes epithelial morphogenesis and is a tumour suppressor, and KIF5B-SYNE4 mediated linkage of MTs to the nucleus is essential for EMT following loss of JAM3, KIF5B and/or SYNE4 may be oncogenes. Indeed tumours with low JAM3 expression have high levels of KIF5B and SYNE4, whereas cells with high levels of JAM3 have low KIF5B and SYNE4 expression (Figure 9D). Moreover, increased KIF5B and

SYNE4 copy numbers were observed in tumours with low JAM3 expression (Figure 9E). Finally, increased KIF5B and SYNE4 expression predicted shorter disease-specific survival periods (Figure 9F). Thus KIF5B and SYNE4 are oncogenes that antagonize the actions of the JAM3 tumour suppressor in patients.

Discussion

During the development and homeostasis of tissues such as the mammalian epidermis, epithelial cells establish apicobasal polarity, form extensive cell-cell contacts, downregulate the formation of focal adhesions (FAs); all which lead to a hexagonal, cube-like cell shapes. Dysregulation of epithelial tissue morphogenesis, such as caused by defects in cell-cell adhesion formation[60-62] and/or loss of apicobasal polarity[6, 63-66] can trigger transcriptional programmes, such as EMT[2], and promote cancer relevant behaviours such as proliferation, invasion, stemness, and drug-resistance[5]. Despite the importance of EMT in tumour progression and metastasis, the mechanistic basis for how a complex series of transcriptional events in the nucleus are regulated by changes in cell shape is very poorly understood. We show that disruption of normal cell-cell adhesion results in alteration in MT organization that can in turn deform nuclei, and upregulate the activity of pro-EMT transcriptional co-activators such as YAP/TAZ. These data provide a mechanistic basis for classic observations, such as those made by Elizabeth Hay[10], that disrupting cell-cell adhesion can promote EMT. Moreover, these data describe a mechanism to explain how loss of cell-cell adhesion, can drive EMT in breast cancer cells [67].

More generally, our results point to an important role for MT reorganization, in the absence of FA maturation and actin reorganization, in promoting YAP and TAZ activation through distorting nuclear shape. Potentially alterations in nuclear shape may affect the conformation of nuclear pore complexes that allow YAP and TAZ to enter the nucleus[19]. Although we observe that JAM3 depletion leads to both YAP and TAZ activation, and that Collagen-I upregulation is dependent on YAP, invasion of JAM3 depleted cells in 3D matrices is dependent solely on TAZ. These observations are remarkably consistent with those observing that induction of Cancer Stem Cell (CSC) programmes in breast cancer cells is dependent on TAZ, but not YAP[67]. Thus we propose that EMT following depletion of JAM3 is dependent on TAZ, but that YAP may also contribute to important changes from the epithelial to mesenchymal states, such as Collagen-I production. MT-mediated regulation of TAZ activation may be a general mechanism in a wide variety of cell types.

Many cancer cells, and normal cells in mesenchymal states such as fibroblasts, have both radial arrays and deformed nuclei[14, 17, 28] suggesting that the combination of MTs and deformable nuclei promotes EMT across a number of contexts, such as those that have poor cell-cell adhesions. The most parsimonious explanation for how alteration of cell-cell adhesion results in MT reorganization, is that components of cell-cell adhesion complexes, such as JAM3, are essential to capture and stabilize MTs, or even nucleate the polymerization of new MTs. Thus depletion of JAM3 results in detachment of MTs from the cell-cell adhesion complexes, and a "collapse" of MTs into a radial structure. Indeed JAM-A, which is highly related to JAM3 has been shown to bind the polarity proteins Par-3[68, 69], and Par-3 is critical for recruitment of MT nucleators such as gamma-tubulin to the apical membrane[70]. How the MTs can make such large deformations in nuclear structure remain to be understood. Because MT plus-ends can still be coupled to the nucleus via KIF5B-SYNE4 complexes, MT polymerization/growth at plus-ends may generate forces that deform the nucleus. Alternatively, the forces may be a consequence of MT-bound motors such a kinesin or dynein[26]. In support of this idea, inhibiting the binding of Kinesin-1 to MTs by RBL rescues nuclear morphology in JAM3 deficient cells, and Kinesin-1 activity is required for nuclear deformation during constricted migration of *C. elegans* P-cells[71], and nuclear rotation during neuronal migration[72]. Thus the motor function of Kkinesin-1 may be responsible for force generation on the nucleus.

Our observations, taken together with extensive previous work on Kinesin-1, suggest that Kinesin-1 function in nuclear morphogenesis differs based on cell type and the organization of the MT array. In epithelial cells, Kinesin-1 serves to physically couple SUN-KASH complexes to MT plus-end[49] (Figure 10). This coupling alone, and/or because of Kinesin-1 ATPase activity, positions nuclei and acts largely to prevent nuclear deformation. In contrast, in mesenchymal cells Kinesin-1 activity contributes to nuclear deformation (Figure 10). We propose that it is likely that Kinesin-1 that is not coupled to the nuclear envelope is also being transported to MT plus ends at the leading edge of cells where it may deliver cargos that facilitate cell invasion[73, 74]. Thus altering MT organization facilitates EMT in large part by switching the effects of Kinesin-1 activity and subcellular localization.

In vivo, JAM3 deficient cells are rounder and larger than JAM3 sufficient counterparts, whereas on stiff tissue culture plastic JAM3 deficient cells are more deformed that wild-type cells. We propose the effects of differential substrate elasticities can explain such differences. JAM3 deficiency, concomitant decreases in the amount LMNA incorporated into the nuclear lamina, and changes in the LMNA:LMNB ratio, results in nuclei that are highly malleable[51, 75]. Because of the stiffness of tissue culture plastic, the reorganized MTS are

capable of generating sufficient force to deform the nucleus. Although malleable, JAM3 depleted nuclei are less elastic, and maintain a “donut/crescent” morphology (similar to paperclip, JAM3 nuclei are malleable but not elastic). But *in vivo* where forces on the nucleus are considerably lower [76], MTs, regardless of their organization, are not capable of deforming the nuclei, and the nuclei of JAM3 sufficient cells *in vivo* retains their shape even after deformation. Thus, while our data strongly support a role for JAM3 in regulating nuclear morphogenesis *in vivo* and in cell culture, caution must be exercised in comparing nuclear shapes between these two settings.

Importantly, our results open up a new avenue for breast cancer treatment. Uncoupling MTs from the nucleus in mesenchymal cells results in downregulation of the EMT programme, prevents invasion, and remodelling of the ECM – but has little effect on cell survival. Thus uncoupling MT-nuclear connections and/or inhibiting Kinesin-1 activity may be suitable as part of differentiation-therapies – which aim not to kill mesenchymal/stem-like/drug-resistance cancer cells directly, but to revert them to an epithelial state which is less aggressive and/or more treatable with conventional therapeutics. In fact, given the prevalence of nuclear pleomorphism in other cancers, and other diseases, targeting MTs and MT-nuclear complexes may be a broadly applicable therapeutic strategy.

Author Contributions

M.G.-A, Y.Y., and C.B. designed the research. M.G.-A performed MCF10A experiments and analyzed all experimental data. Y.Y. performed the bioinformatic analysis. R.R. Performed the sub fractionation experiments. J.E.S. wrote the script to segment donut nuclei. M.G.-A, Y.Y., and C.B. wrote the manuscript.

Acknowledgements

We thank F. Wallberg for assistance with image analysis and R. Patel for cytometry help (Flow Cytometry and Light Microscopy Facility, ICR, London, UK). We also thank A. Sadok (Cancer Therapeutics, ICR, London, UK) for technical help in bottom to top invasion assays. We thank J. Mansfield (TU-Dresden) for the MCF10A-PCNA cell line. We are grateful to Lucas Dent (ICR) for comments on the manuscript. This project was initiated by Y.Y. in the laboratory of Florian Markowetz (Cancer Research UK Cambridge Institute). Y.Y. is supported by a Cancer Research UK Career Establishment Award (C45982/A21808), Breast Cancer Now (2015NovPR638), NIH U54 CA217376, R01 CA185138, CDMRP Breast Cancer Research Program Award BC132057, Wellcome Trust (105104/Z/14/Z), and The Royal Marsden/ICR National Institute of Health Research Biomedical Research Centre. C.B. is supported by a Stand Up to Cancer UK Programme Foundation Award (C37275/1, A20146) and a CRUK/EPSRC Multidisciplinary Research Award (NS/A000062/1).

Figure Legends

Figure 1. Computational pipeline for the integrative analysis of morphological and molecular data in human breast tumours.

(A) Automated image analysis enables identification of three cell types and quantification of morphological features from an H&E whole tumour section. The distribution of each morphological feature for all cancer nuclei in a tumour image can be summarized using statistical descriptors: median, standard deviation, and skewness. These morphological scores can then represent tumour morphological profiles, which are then associated with genomic aberrations, gene expression data and patient prognosis.

(B) Morphology-Expression hybrid Network representing significant associations between 18 cancer nuclear morphology scores and 1,000 cis-acting genes (feature name sd g.ecc: standard deviation of geometric eccentricity; median m.ecc: median value of moment eccentricity). (C) Illustrative examples of cancer nuclei with high and low value of image moment I1. (D) Illustrative examples of tumours with high and low CNI.

Figure 2. JAM3 as a potential driver of morphological heterogeneity.

(A) Heatmap of RNA expression of genes with highest positive correlation with CNI, samples were annotated with intrinsic subtypes. (B) Boxplot showing the difference in JAM3 gene expression according to JAM3 DNA copy number status. (C) Boxplot showing the difference in JAM3 gene expression according to intrinsic subtypes. (D) Boxplot showing the difference in JAM3 gene expression according to the 10 integrative subtypes. (E) Boxplot showing the difference in JAM3 gene expression according to two main histology subtypes. IDC: Invasive Ductal Carcinoma; ILC: Invasive Lobular Carcinoma. (F) Boxplot showing the difference in JAM3 gene expression according to tumour grades.

Figure 3. JAM-3 regulates nuclear and microtubule organization in epithelial cells.

(A) Control or JAM3-depleted cells were labelled with Hoechst (blue) and immunostained for JAM-3 (green), alpha-tubulin (red) or beta-catenin (green). Scale bars, 20um. (B) Representative images of the 'donut' nuclei (blue; labelled with Hoescht) and the microtubules (red; immunostained with alpha-tubulin) characteristic of MCF10A cells transfected with 2 different siRNAs targeting JAM3. Scale bars, 50um. (C, D) Quantification of perinuclear alpha tubulin intensity (C) and percentage of cells with nuclear donuts (D) in control and JAM-3 depleted cells. Graph shows the representative data of 3 different experiments ($n > 12.000$ cells). Comparisons among groups were performed by one-way ANOVA (Newman-Keuls multiple comparison test; $*p < 0.05$, $**p < 0.01$, $***p < 0.001$, $****p < 0.0001$). (E,F) MCF10A cells were allowed to invade "upward" into a Bovine

Collagen I matrix, fixed, and labelled with Phalloidin (green) and Hoescht (blue), and then imaged at three different planes. (E) On the left is the invasion index of control and JAM3 depleted MCF10A cells. Representative data from 2 different experiments (n > 5.000 cells). Comparisons among groups were performed by one-way ANOVA (Newman-Keuls multiple comparison test; $*p < 0.05$, $**p < 0.01$, $***p < 0.001$, $****p < 0.0001$). Right shows representative images of cells in the 3 different planes imaged at 0, 30 and 60um. Scale bars, 50um (F) Left panel shows the invasion index of control and JAM3 depleted MCF10A cells treated with DMSO or MMP inhibitor GM6001. Graph shows the data of two different experiments (n > 5.000 cells). Comparisons among groups were performed by one-way ANOVA (Newman-Keuls multiple comparison test; $*p < 0.05$, $**p < 0.01$, $***p < 0.001$, $****p < 0.0001$). Right panel shows representative images of cells in the 3 different invasion planes imaged at 0, 30 and 60um. Scale bars, 50um (G) Heat map showing relative gene expression panel after treating MCF10A cells with 3 different siRNAs targeting JAM3.

Figure 4. JAM3 is required for the morphogenesis of epithelial morphogenesis in 3D. (A,B) MCF10A Control or JAM3-depleted cells by 2 different siRNAs growing in a Matrigel:Collagen thick matrix, allowed to form acini for 2 days, fixed and inmunostained. (A) Maximum projection of representative images of acini labelled with Hoechst (blue) and inmunostained for phalloidin (green), Laminin5 (red) and Fibronectin (white). Scale bars, 50um. (B) Graphs showing the morphology features of the 3 conditions. The majority of the structures formed had 2 or more nuclei, hence considered as Acini. Area was normalized to the Control. F-actin protrusions of the acini were described as Number of neurites and normalized to the control. Fibronectin intensity of the acini was expressed as the mean fibronectin intensity of the whole acini divided by the area of the acini and normalized to the Control. Data shows the result of one experiment where 4 wells per condition were analysed (n > 200 acini per condition). Comparisons among groups were performed by one-way ANOVA (Dunnett´s multiple comparison test) with Prism6 software ($*p < 0.05$, $**p < 0.01$, $***p < 0.001$, $****p < 0.0001$). (C,D) Visual quantification of the number of structures forming normal (round) or abnormal (irregular shape, multiple lobules or protrusive acini) acini at day 8 and expressed as a percentage (n = 100 acini). t student was performed with Prism6 software ($*p < 0.05$, $**p < 0.01$, $***p < 0.001$, $****p < 0.0001$). (D) Confocal sections of Control or JAM3-depleted MCF10A acini in a Matrigel:Collagen mix, 4 days or 8 days after transfection and labelled with Phalloidin (green), Laminin5 (red) and Hoeschst (blue). Scale bars indicated in the figures.

Figure 5. JAM3 depletion results in nuclear translocation of the YAP and TAZ transcription factors. (A) Quantification of the nuclear:cytoplasmic YAP or TAZ ratios for wild-type and JAM3-depleted cells (n > 15.000 cells). Data shows the results of 3 different experiments. Comparisons among groups were performed by one-way ANOVA (Newman-Keuls multiple comparison test) with Prism6 software (∗p < 0.05, ∗∗p < 0.01, ∗∗∗p < 0.001, ∗∗∗∗p < 0.0001). (B) Wild-type and JAM3-depleted cells were labelled with Hoechst (blue) and inmunostained for TAZ (green), YAP (red) and alpha tubulin (yellow). Scale bars, 50um. (C) YAP and TAZ nuclear:cytoplasmic ratio as determined by biochemical fractionation in control and siJAM3 depleted (siG RNAi) cells. (D) Percentage of YAP or TAZ in cytoplasm, membrane, nuclear soluble, chromatin-bound and cytoskeletal protein extracts in wild-type and JAM3-depleted cells as determined by biochemical fractionation. Pie charts represents the percentage of YAP and TAZ protein localization in each fraction determined by WB of the different extracts. Data shows the result of one experiment where 1.000.000 cells were lysed per condition. (E) Relative mRNA levels of CTGF, JAM3, YAP and TAZ normalized to GAPDH for wild-type and JAM3, YAP, or TAZ depleted cells. Mean ± SD (n = 3 replicates/condition).

Figure 6. TAZ is required for EMT in 3D. (A,B) MCF10A Control or JAM3-depleted cells alone or in combination with YAP or TAZ siRNAs were plated in a Matrigel:Collagen thick matrix, allowed to form acini for 2 days, fixed and stained. (A) Maximum projection of representative images of acini labelled with Hoechst (blue) and phalloidin (green). Scale bars, 50um. (B) Graphs showing the morphology features of the 4 conditions. Fibronectin intensity of the acini was expressed as the mean fibronectin intensity of the whole acini divided by the area of the acini and normalized to the Control. F-actin protrusions of the acini were described as Number of neurites per acini and also their length was measured and normalized to the control. Data shows the result of two independent experiments where at least 2 wells per condition were analysed (n > 150 acini per condition). Comparisons among groups were performed by one-way ANOVA (Dunnett´s multiple comparison test) with Prism6 software (∗p < 0.05, ∗∗p < 0.01, ∗∗∗p < 0.001, ∗∗∗∗p < 0.0001).

Figure 7. Uncoupling the nucleus and microtubules prevents EMT following JAM3 depletion. (A) Percentage of cells with nuclear donuts and (B) quantification of Intensity of perinuclear alpha tubulin in cells treated with JAM3 siRNA alone, or in combination with a panel of siRNAs targeting almost all the LINC components (n > 4.000 cells). Comparisons among groups were performed by one-way ANOVA (Newman-Keuls multiple comparison test) with Prism6 software (∗p < 0.05, ∗∗p < 0.01, ∗∗∗p < 0.001, ∗∗∗∗p < 0.0001). (C) Representative images of the nuclei (blue, Hoechst) and the MTOC (red, alpha tubulin) of

MCF10A cells transfected with a panel of siRNAs targeting several LINC components alone or in combination with JAM3. Scale bars, 50um. (D) Invasion index of MCF10A cells into a Bovine Collagen I matrix depleted of single genes, or genes in combination. Graphs show the representative data of 2 different experiments (n > 5.000 cells). Comparisons among groups were performed by one-way ANOVA (Newman-Keuls multiple comparison test) with Prism6 software (∗p < 0.05, ∗∗p < 0.01, ∗∗∗p < 0.001, ∗∗∗∗p < 0.0001). (E) Relative mRNA levels of CTGF normalized to GAPDH for wild-type, JAM3 depleted, KIF5B+SYNE4 depleted, and Triple knockdown cells. Mean ± SD (n = 3 replicates/condition). (∗p < 0.05, ∗∗p < 0.01). (F-H) Wild-type, JAM3-depleted cells single or in combination with KIF5B and/or SYNE4 RNAi were labelled with Hoechst (blue) and inmunostained for TAZ (green), YAP (red) and alpha tubulin (yellow). (F) Quantification of the nuclear/cytoplasmic YAP ratio after the RNAi treatments. (G) Quantification of the nuclear/cytoplasmic TAZ ratio after the RNAi treatments. (n>15.000 cells). Data shows the results of 3 different experiments. Comparisons among groups were performed by one-way ANOVA (Newman-Keuls multiple comparison test) with Prism6 software (∗p < 0.05, ∗∗p < 0.01, ∗∗∗p < 0.001). (H) Representative images of the wild-type, JAM3 and Triple depleted cells. Scale bars, 50um. (I) YAP and TAZ nuclear:cytoplasmic ratio as determined by biochemical fractionation in wild-type, JAM3 and Triple depleted cells. (J) YAP and TAZ subcellular localization as determined by biochemical fractionation in control, JAM3 depleted, and triple knockdown cells. Pie charts represent the percentage of YAP and TAZ protein localization in each fraction determined by WB of the different extracts for each RNAi treatment. Data shows the result of one experiment where 1.000.000 cells were lysed per condition.

Figure 8. Nuclear morphology defects observed following JAM3 depletion are due to changes in the levels of LMNA and/or LMNB in the nuclear membrane. (A,B) (A) Percentage of cells with nuclear donuts after LMNA or LMNB depletion alone or in combination with JAM-3 (n > 15,000 cells). Data shows the results of 3 different experiments. Comparisons among groups were performed by one-way ANOVA (Newman-Keuls multiple comparison test) with Prism6 software (∗p < 0.05, ∗∗p < 0.01, ∗∗∗p < 0.001, ∗∗∗∗p < 0.0001). (B) Nuclei of the cells in (A) labelled with Hoechst (blue). Arrows indicate donut nuclei. Scale bars, 50um. (C-E) MCF10A cells treated with different siRNAs and inmunostained with LMNA and LMNB. (C) Panel of images showing the co-staining of LMNA (green) and LMNB (red) after the RNAi treatments. Scale bars, 20 um. (D) Quantification of the LMNA intensity in the Outer nuclear membrane/inner nuclei and normalized to the Control value. (E) Quantification of the LMNB intensity in the Outer nuclear membrane/inner nuclei and normalized to the Control value. (n>15.000 cells). Data shows

the results of 2 different experiments. Comparisons among groups were performed by one-way ANOVA (Newman-Keuls multiple comparison test) with Prism6 software (∗p < 0.05, ∗∗p < 0.01, ∗∗∗p < 0.001, ∗∗∗∗p < 0.0001). (F) LMNA and LMNB intensity levels in the Outer Nuclear membrane of wild-type, JAM3 and Triple depleted cells. Comparisons among groups were performed by one-way ANOVA (Newman-Keuls multiple comparison test) with Prism6 software (∗p < 0.05, ∗∗p < 0.01, ∗∗∗p < 0.001, ∗∗∗∗p < 0.0001). (G) Cells were depleted of JAM3 alone, or in combination with KIF5B and/or SYNE4, and labelled with Hoechst, LMNA, phospho-LMNA and alpha tubulin. Images (left panel) show cells stained with Hoechst (blue) and immunostained for LMNA (green), phospho-LMNA (red) and alpha tubulin (white). Scale bars, 20um. Graph (right) shows the quantification of the ratio of phosphoLMNA in the inner nuclei or nucleoplasm/ LMNA in the Outer membrane after the RNAi treatments. Graphs shows the representative data of 2 different experiments (n > 5.000 cells). Comparisons among groups were performed by one-way ANOVA (Newman-Keuls multiple comparison test) with Prism6 software (∗p < 0.05, ∗∗p < 0.01, ∗∗∗p < 0.001, ∗∗∗∗p < 0.0001).

Figure 9. JAM-3 loss drives tumorigenesis and metastasis in breast cancer patients. (A-B) Kaplan-Meier curves illustrating the difference in disease-specific survival over 10 years according to JAM3 gene expression in different subtypes within METABRIC and in Luminal A subtypes of an independent cohort. ILC: Invasive Lobular Carcinoma. Within the luminal A subtype that had large number of samples, patients were spilt into equal-sized groups. For ILC and the Normal subtype, a best cut-off point was identified by testing different cut-offs. (C) Fold change in frequency of metastasis stratified by JAM3 copy number status. (D) Correlation between KIF5B/SYNE4 expression and JAM3 expression. (E) Boxplots illustrating the difference in JAM3 gene expression according to the copy number status of KIF5B and SYNE4. (F) Kaplan-Meier curves illustrating the difference in disease-specific survival over 10 years according to KIF5B/SYNE4 gene expression in different subtypes within METABRIC.

Figure10. Model for EMT driven by JAM3 depletion. In wild-type (WT) epithelial cells, the MT are organized such that minus ends are anchored at cell-cell adhesion by JAM3. MT plus ends are anchored at the nuclear membrane by KIF5B-SYNE4 complexes. In this configuration the nucleus is cushioned from deformation, and both YAP and TAZ are deactivated. In JAM3 deficient cells, MTs are reorganized into radial arrays. This confirmation results in nuclear deformation by the MTs, loss of LMNA from the membrane,

increased LMNA phosphorylation, “softening” of the nucleus, translocation of YAP and TAZ into the nucleus, and upregulation of EMT genes.

References

1. Thiery, J.P., Acloque, H., Huang, R.Y. & Nieto, M.A. Epithelial-mesenchymal transitions in development and disease. *Cell* **139**, 871-890 (2009).
2. Nieto, M.A., Huang, R.Y., Jackson, R.A. & Thiery, J.P. Emt: 2016. *Cell* **166**, 21-45 (2016).
3. Kroger, C. *et al.* Acquisition of a hybrid E/M state is essential for tumorigenicity of basal breast cancer cells. *Proc Natl Acad Sci U S A* (2019).
4. Mani, S.A. *et al.* The epithelial-mesenchymal transition generates cells with properties of stem cells. *Cell* **133**, 704-715 (2008).
5. Dongre, A. & Weinberg, R.A. New insights into the mechanisms of epithelial-mesenchymal transition and implications for cancer. *Nat Rev Mol Cell Biol* **20**, 69-84 (2019).
6. Zhan, L. *et al.* Deregulation of scribble promotes mammary tumorigenesis and reveals a role for cell polarity in carcinoma. *Cell* **135**, 865-878 (2008).
7. Paszek, M.J. *et al.* Tensional homeostasis and the malignant phenotype. *Cancer Cell* **8**, 241-254 (2005).
8. Levental, K.R. *et al.* Matrix crosslinking forces tumor progression by enhancing integrin signaling. *Cell* **139**, 891-906 (2009).
9. Gomez, E.W., Chen, Q.K., Gjorevski, N. & Nelson, C.M. Tissue geometry patterns epithelial-mesenchymal transition via intercellular mechanotransduction. *Journal of cellular biochemistry* **110**, 44-51 (2010).
10. Greenburg, G. & Hay, E.D. Epithelia suspended in collagen gels can lose polarity and express characteristics of migrating mesenchymal cells. *J Cell Biol* **95**, 333-339 (1982).
11. Starr, D.A. & Fridolfsson, H.N. Interactions between nuclei and the cytoskeleton are mediated by SUN-KASH nuclear-envelope bridges. *Annu Rev Cell Dev Biol* **26**, 421-444 (2010).
12. Simon, D.N. & Wilson, K.L. The nucleoskeleton as a genome-associated dynamic 'network of networks'. *Nat Rev Mol Cell Biol* **12**, 695-708 (2011).
13. Swift, J. & Discher, D.E. The nuclear lamina is mechano-responsive to ECM elasticity in mature tissue. *J Cell Sci* **127**, 3005-3015 (2014).
14. Dahl, K.N., Ribeiro, A.J. & Lammerding, J. Nuclear shape, mechanics, and mechanotransduction. *Circulation research* **102**, 1307-1318 (2008).
15. Cho, S., Irianto, J. & Discher, D.E. Mechanosensing by the nucleus: From pathways to scaling relationships. *J Cell Biol* **216**, 305-315 (2017).
16. Kirby, T.J. & Lammerding, J. Emerging views of the nucleus as a cellular mechanosensor. *Nat Cell Biol* **20**, 373-381 (2018).
17. Dauer, W.T. & Worman, H.J. The nuclear envelope as a signaling node in development and disease. *Dev Cell* **17**, 626-638 (2009).
18. Sero, J.E. *et al.* Cell shape and the microenvironment regulate nuclear translocation of NF-kappaB in breast epithelial and tumor cells. *Molecular systems biology* **11**, 790 (2015).
19. Elosegui-Artola, A. *et al.* Force Triggers YAP Nuclear Entry by Regulating Transport across Nuclear Pores. *Cell* **171**, 1397-1410 e1314 (2017).
20. Butin-Israeli, V., Adam, S.A., Goldman, A.E. & Goldman, R.D. Nuclear lamin functions and disease. *Trends Genet* **28**, 464-471 (2012).
21. Bartolini, F. & Gundersen, G.G. Generation of noncentrosomal microtubule arrays. *J Cell Sci* **119**, 4155-4163 (2006).
22. Meads, T. & Schroer, T.A. Polarity and nucleation of microtubules in polarized epithelial cells. *Cell Motil Cytoskeleton* **32**, 273-288 (1995).
23. Akhmanova, A. & Hoogenraad, C.C. Microtubule minus-end-targeting proteins. *Curr Biol* **25**, R162-171 (2015).
24. Keating, T.J. & Borisy, G.G. Centrosomal and non-centrosomal microtubules. *Biol Cell* **91**, 321-329 (1999).

25. Shtutman, M. *et al.* Signaling function of alpha-catenin in microtubule regulation. *Cell Cycle* **7**, 2377-2383 (2008).
26. Wang, S., Reuveny, A. & Volk, T. Nesprin provides elastic properties to muscle nuclei by cooperating with spectraplakin and EB1. *J Cell Biol* **209**, 529-538 (2015).
27. Chow, K.H., Factor, R.E. & Ullman, K.S. The nuclear envelope environment and its cancer connections. *Nature reviews. Cancer* **12**, 196-209 (2012).
28. Bussolati, G. Proper detection of the nuclear shape: ways and significance. *Romanian journal of morphology and embryology = Revue roumaine de morphologie et embryologie* **49**, 435-439 (2008).
29. Krause, M. & Wolf, K. Cancer cell migration in 3D tissue: negotiating space by proteolysis and nuclear deformability. *Cell adhesion & migration* **9**, 357-366 (2015).
30. Takaki, T. *et al.* Actomyosin drives cancer cell nuclear dysmorphia and threatens genome stability. *Nature communications* **8**, 16013 (2017).
31. Xia, Y. *et al.* Nuclear rupture at sites of high curvature compromises retention of DNA repair factors. *J Cell Biol* **217**, 3796-3808 (2018).
32. Irianto, J. *et al.* DNA Damage Follows Repair Factor Depletion and Portends Genome Variation in Cancer Cells after Pore Migration. *Curr Biol* **27**, 210-223 (2017).
33. Bakhoum, S.F. *et al.* Chromosomal instability drives metastasis through a cytosolic DNA response. *Nature* **553**, 467-472 (2018).
034. Curtis, C. *et al.* The genomic and transcriptomic architecture of 2,000 breast tumours reveals novel subgroups. *Nature* **486**, 346-352 (2012).
35. Choy, B., LaLonde, A., Que, J., Wu, T. & Zhou, Z. MCM4 and MCM7, potential novel proliferation markers, significantly correlated with Ki-67, Bmi1, and cyclin E expression in esophageal adenocarcinoma, squamous cell carcinoma, and precancerous lesions. *Human pathology* **57**, 126-135 (2016).
36. Baxley, R.M. & Bielinsky, A.K. Mcm10: A Dynamic Scaffold at Eukaryotic Replication Forks. *Genes* **8** (2017).
37. Gartel, A.L. FOXM1 in Cancer: Interactions and Vulnerabilities. *Cancer research* **77**, 3135-3139 (2017).
38. Yasmeen, A., Berdel, W.E., Serve, H. & Muller-Tidow, C. E- and A-type cyclins as markers for cancer diagnosis and prognosis. *Expert review of molecular diagnostics* **3**, 617-633 (2003).
39. Marzec, K. & Burgess, A. The Oncogenic Functions of MASTL Kinase. *Frontiers in cell and developmental biology* **6**, 162 (2018).
40. Bakal, C., Aach, J., Church, G. & Perrimon, N. Quantitative morphological signatures define local signaling networks regulating cell morphology. *Science* **316**, 1753-1756 (2007).
41. Economopoulou, M. *et al.* Expression, localization, and function of junctional adhesion molecule-C (JAM-C) in human retinal pigment epithelium. *Invest Ophthalmol Vis Sci* **50**, 1454-1463 (2009).
42. Zen, K. *et al.* JAM-C is a component of desmosomes and a ligand for CD11b/CD18-mediated neutrophil transepithelial migration. *Mol Biol Cell* **15**, 3926-3937 (2004).
43. Lamagna, C. *et al.* Dual interaction of JAM-C with JAM-B and alpha(M)beta2 integrin: function in junctional complexes and leukocyte adhesion. *Mol Biol Cell* **16**, 4992-5003 (2005).
44. Aurrand-Lions, M., Johnson-Leger, C., Wong, C., Du Pasquier, L. & Imhof, B.A. Heterogeneity of endothelial junctions is reflected by differential expression and specific subcellular localization of the three JAM family members. *Blood* **98**, 3699-3707 (2001).
45. Shiu, J.Y., Aires, L., Lin, Z. & Vogel, V. Nanopillar force measurements reveal actin-cap-mediated YAP mechanotransduction. *Nat Cell Biol* **20**, 262-271 (2018).
46. Shao, D.D. *et al.* KRAS and YAP1 converge to regulate EMT and tumor survival. *Cell* **158**, 171-184 (2014).
47. Lamar, J.M. *et al.* The Hippo pathway target, YAP, promotes metastasis through its TEAD-interaction domain. *Proc Natl Acad Sci U S A* **109**, E2441-2450 (2012).

48. Overholtzer, M. *et al.* Transforming properties of YAP, a candidate oncogene on the chromosome 11q22 amplicon. *Proc Natl Acad Sci U S A* **103**, 12405-12410 (2006).
49. Roux, K.J. *et al.* Nesprin 4 is an outer nuclear membrane protein that can induce kinesin-mediated cell polarization. *Proc Natl Acad Sci U S A* **106**, 2194-2199 (2009).
50. Buxboim, A. *et al.* Coordinated increase of nuclear tension and lamin-A with matrix stiffness outcompetes lamin-B receptor that favors soft tissue phenotypes. *Mol Biol Cell* **28**, 3333-3348 (2017).
51. Swift, J. *et al.* Nuclear lamin-A scales with tissue stiffness and enhances matrix-directed differentiation. *Science* **341**, 1240104 (2013).
52. Heald, R. & McKeon, F. Mutations of phosphorylation sites in lamin A that prevent nuclear lamina disassembly in mitosis. *Cell* **61**, 579-589 (1990).
53. Buxboim, A. *et al.* Matrix elasticity regulates lamin-A,C phosphorylation and turnover with feedback to actomyosin. *Curr Biol* **24**, 1909-1917 (2014).
54. Hopkins, S.C., Vale, R.D. & Kuntz, I.D. Inhibitors of kinesin activity from structure-based computer screening. *Biochemistry* **39**, 2805-2814 (2000).
55. Fischer, K.R. *et al.* Epithelial-to-mesenchymal transition is not required for lung metastasis but contributes to chemoresistance. *Nature* **527**, 472-476 (2015).
56. Somarelli, J.A. *et al.* Distinct routes to metastasis: plasticity-dependent and plasticity-independent pathways. *Oncogene* **35**, 4302-4311 (2016).
57. Zheng, X. *et al.* Epithelial-to-mesenchymal transition is dispensable for metastasis but induces chemoresistance in pancreatic cancer. *Nature* **527**, 525-530 (2015).
58. Kang, Y. *et al.* A multigenic program mediating breast cancer metastasis to bone. *Cancer Cell* **3**, 537-549 (2003).
59. Esposito, M., Guise, T. & Kang, Y. The Biology of Bone Metastasis. *Cold Spring Harb Perspect Med* **8** (2018).
60. Vasioukhin, V., Bauer, C., Degenstein, L., Wise, B. & Fuchs, E. Hyperproliferation and defects in epithelial polarity upon conditional ablation of alpha-catenin in skin. *Cell* **104**, 605-617 (2001).
61. Kobielak, A. & Fuchs, E. Links between alpha-catenin, NF-kappaB, and squamous cell carcinoma in skin. *Proc Natl Acad Sci U S A* **103**, 2322-2327 (2006).
62. Perez-Moreno, M. & Fuchs, E. Catenins: keeping cells from getting their signals crossed. *Dev Cell* **11**, 601-612 (2006).
63. Martin-Belmonte, F. & Perez-Moreno, M. Epithelial cell polarity, stem cells and cancer. *Nature reviews. Cancer* **12**, 23-38 (2011).
64. Pearson, H.B. *et al.* SCRIB expression is deregulated in human prostate cancer, and its deficiency in mice promotes prostate neoplasia. *J Clin Invest* **121**, 4257-4267 (2011).
65. Bilder, D., Li, M. & Perrimon, N. Cooperative regulation of cell polarity and growth by Drosophila tumor suppressors. *Science* **289**, 113-116 (2000).
66. Bilder, D. & Perrimon, N. Localization of apical epithelial determinants by the basolateral PDZ protein Scribble. *Nature* **403**, 676-680 (2000).
67. Cordenonsi, M. *et al.* The Hippo transducer TAZ confers cancer stem cell-related traits on breast cancer cells. *Cell* **147**, 759-772 (2011).
68. Ebnet, K. *et al.* The cell polarity protein ASIP/PAR-3 directly associates with junctional adhesion molecule (JAM). *The EMBO journal* **20**, 3738-3748 (2001).
69. Itoh, M. *et al.* Junctional adhesion molecule (JAM) binds to PAR-3: a possible mechanism for the recruitment of PAR-3 to tight junctions. *J Cell Biol* **154**, 491-497 (2001).
70. Feldman, J.L. & Priess, J.R. A role for the centrosome and PAR-3 in the hand-off of MTOC function during epithelial polarization. *Curr Biol* **22**, 575-582 (2012).
71. Bone, C.R., Chang, Y.T., Cain, N.E., Murphy, S.P. & Starr, D.A. Nuclei migrate through constricted spaces using microtubule motors and actin networks in C. elegans hypodermal cells. *Development* **143**, 4193-4202 (2016).

72. Wu, Y.K., Umeshima, H., Kurisu, J. & Kengaku, M. Nesprins and opposing microtubule motors generate a point force that drives directional nuclear motion in migrating neurons. *Development* **145** (2018).
73. Wang, Z. *et al.* Binding of PLD2-Generated Phosphatidic Acid to KIF5B Promotes MT1-MMP Surface Trafficking and Lung Metastasis of Mouse Breast Cancer Cells. *Dev Cell* **43**, 186-197 e187 (2017).
74. Marchesin, V. *et al.* ARF6-JIP3/4 regulate endosomal tubules for MT1-MMP exocytosis in cancer invasion. *J Cell Biol* **211**, 339-358 (2015).
75. Lammerding, J. *et al.* Lamin A/C deficiency causes defective nuclear mechanics and mechanotransduction. *J Clin Invest* **113**, 370-378 (2004).
76. Cheng, Q. *et al.* Stiffness of the microenvironment upregulates ERBB2 expression in 3D cultures of MCF10A within the range of mammographic density. *Scientific reports* **6**, 28987 (2016).
77. Yuan, Y. *et al.* Quantitative image analysis of cellular heterogeneity in breast tumors complements genomic profiling. *Science translational medicine* **4**, 157ra143 (2012).
78. Debnath, J., Muthuswamy, S.K. & Brugge, J.S. Morphogenesis and oncogenesis of MCF-10A mammary epithelial acini grown in three-dimensional basement membrane cultures. *Methods* **30**, 256-268 (2003).

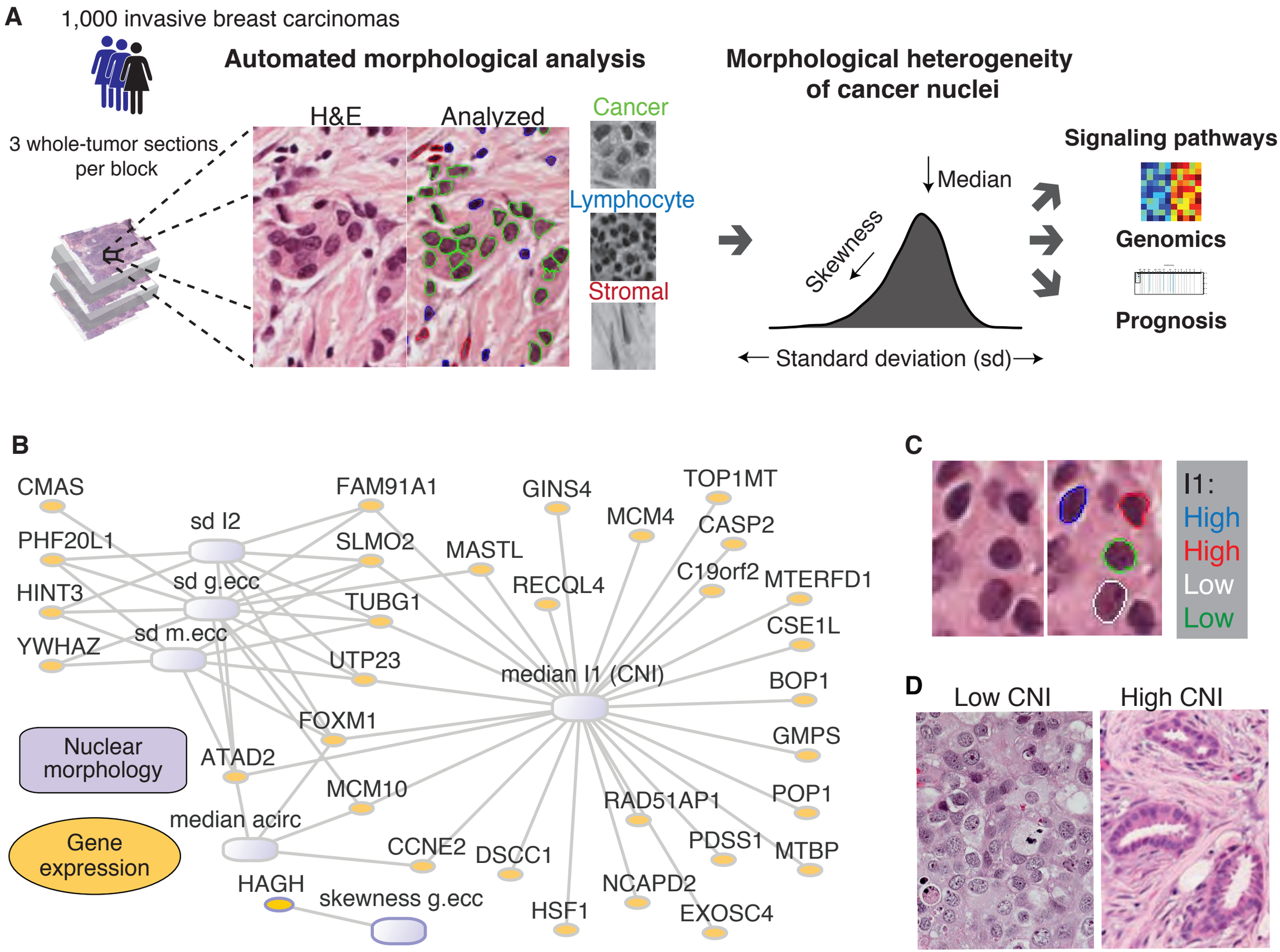

Figure 1. Arias-Garcia et al.

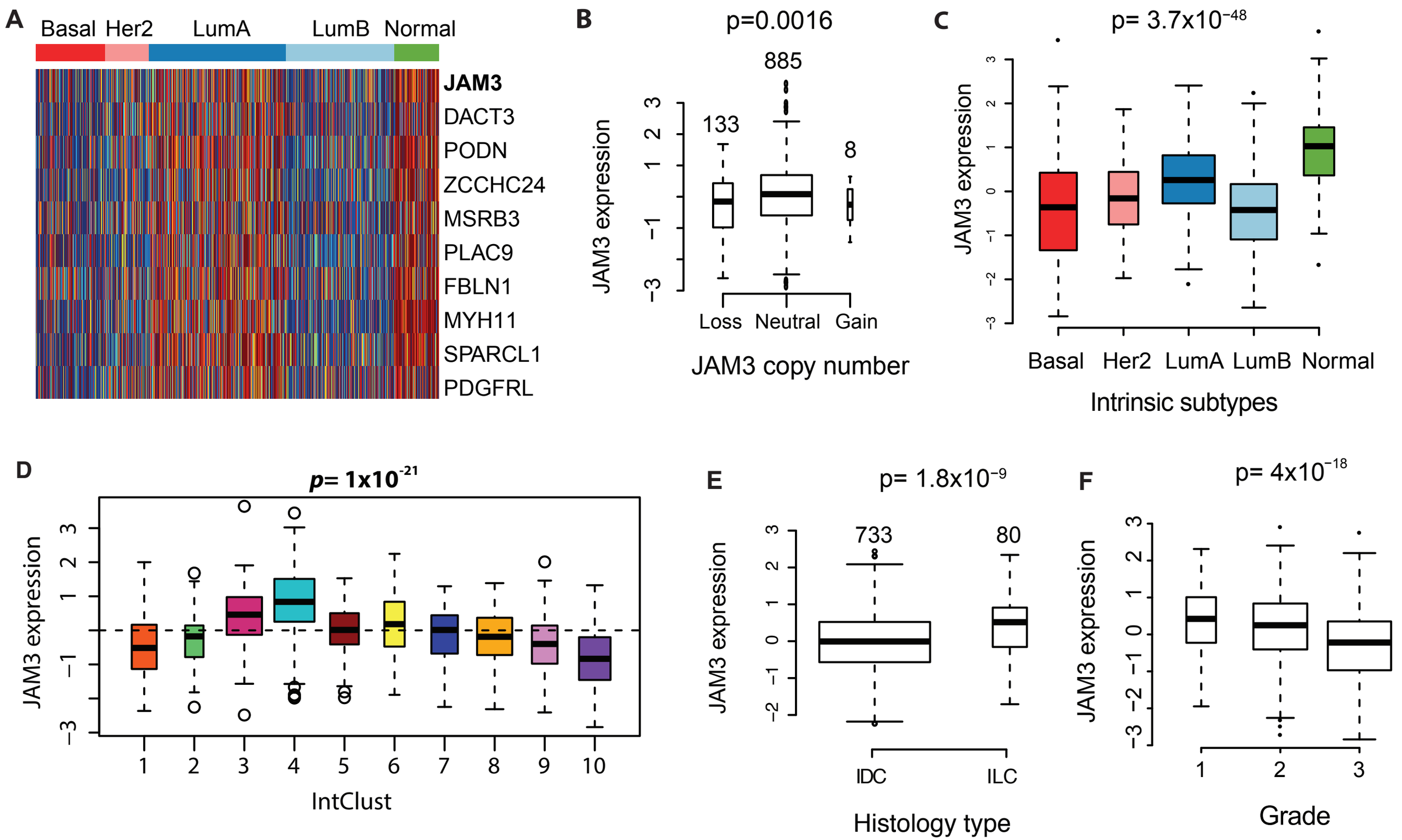

Figure 2. Arias-Garcia et al.

Figure 3. Arias-Garcia et al.

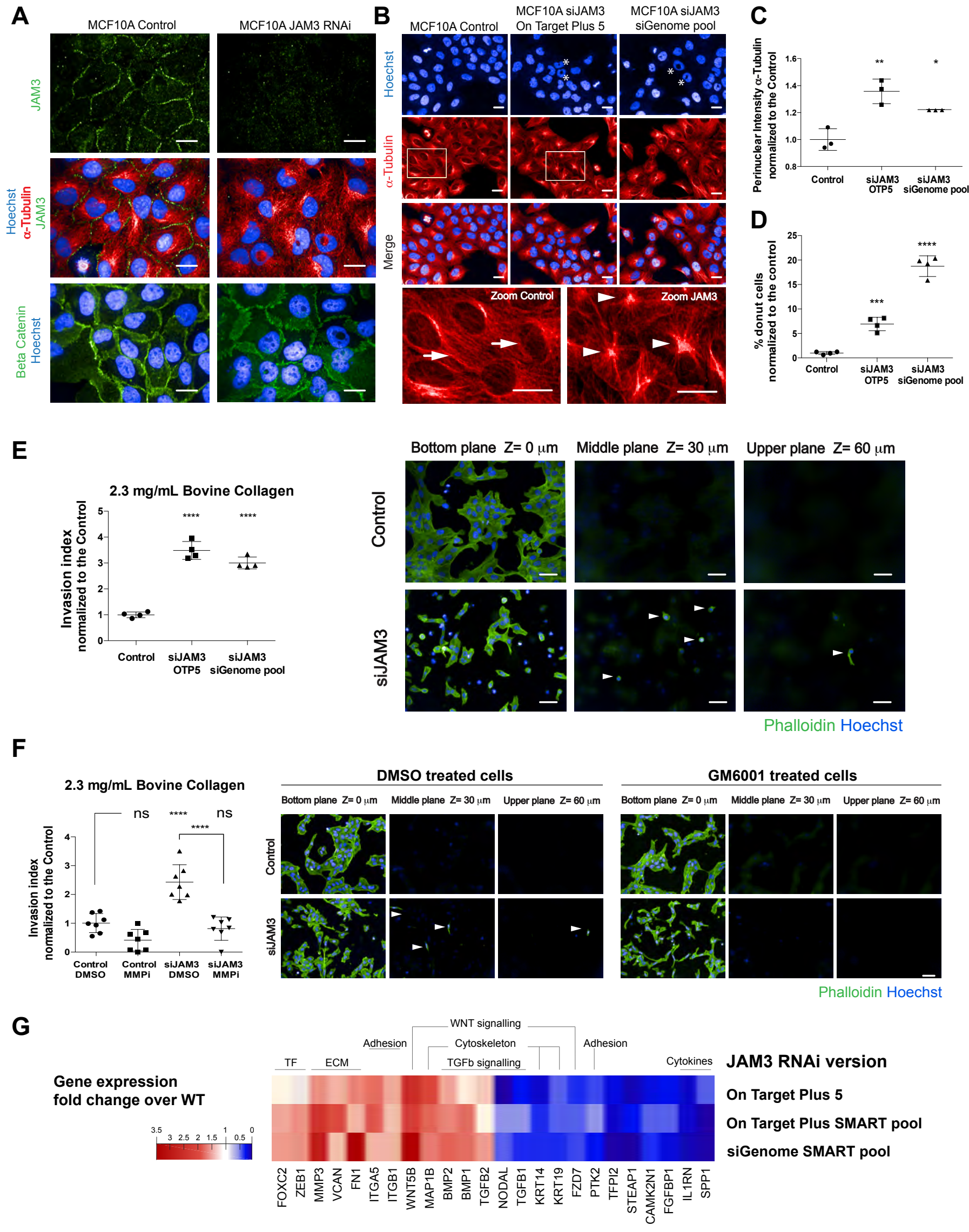

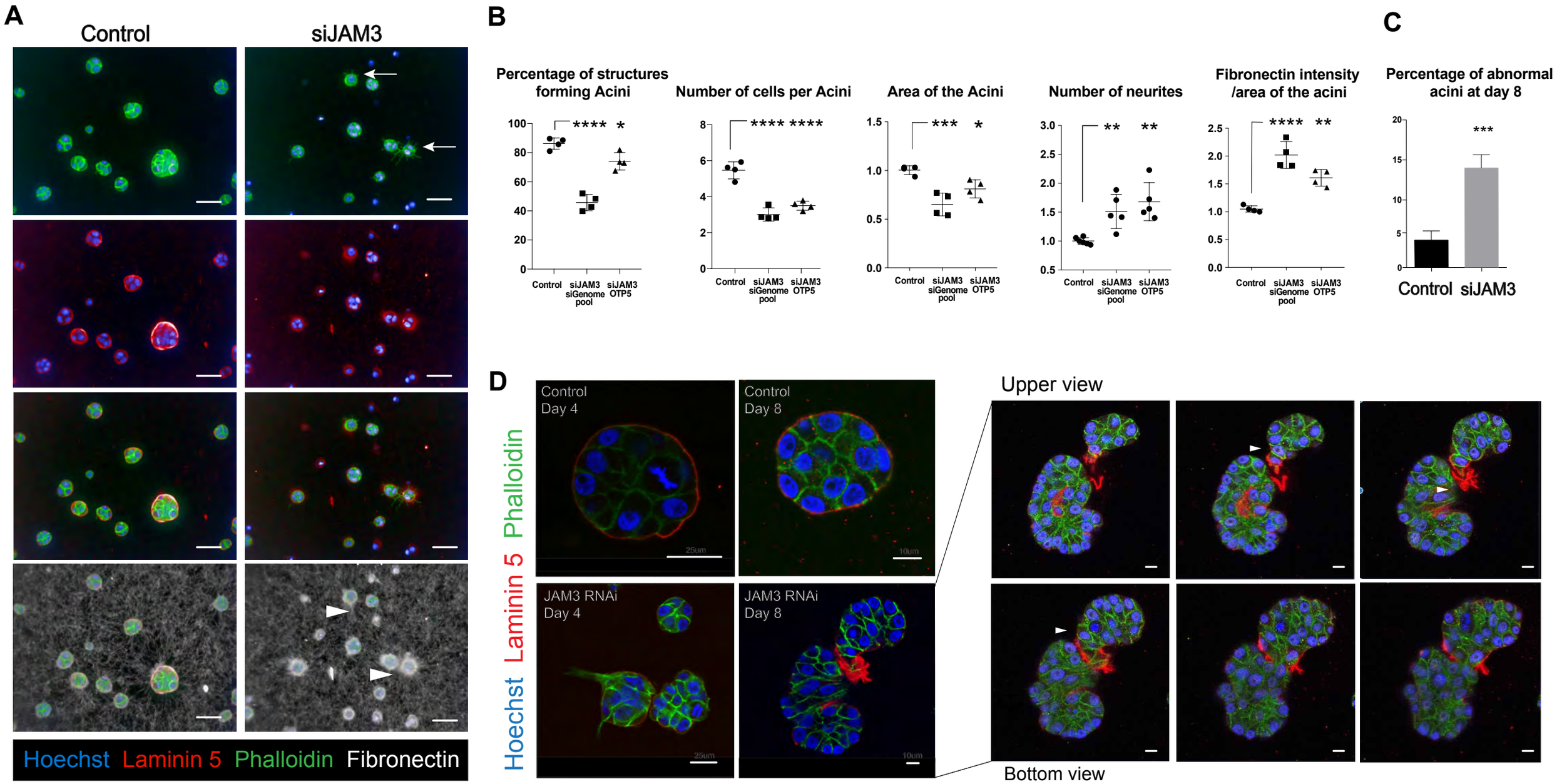

Figure 4. Arias-Garcia et al.

Figure 5. Arias-Garcia et al.

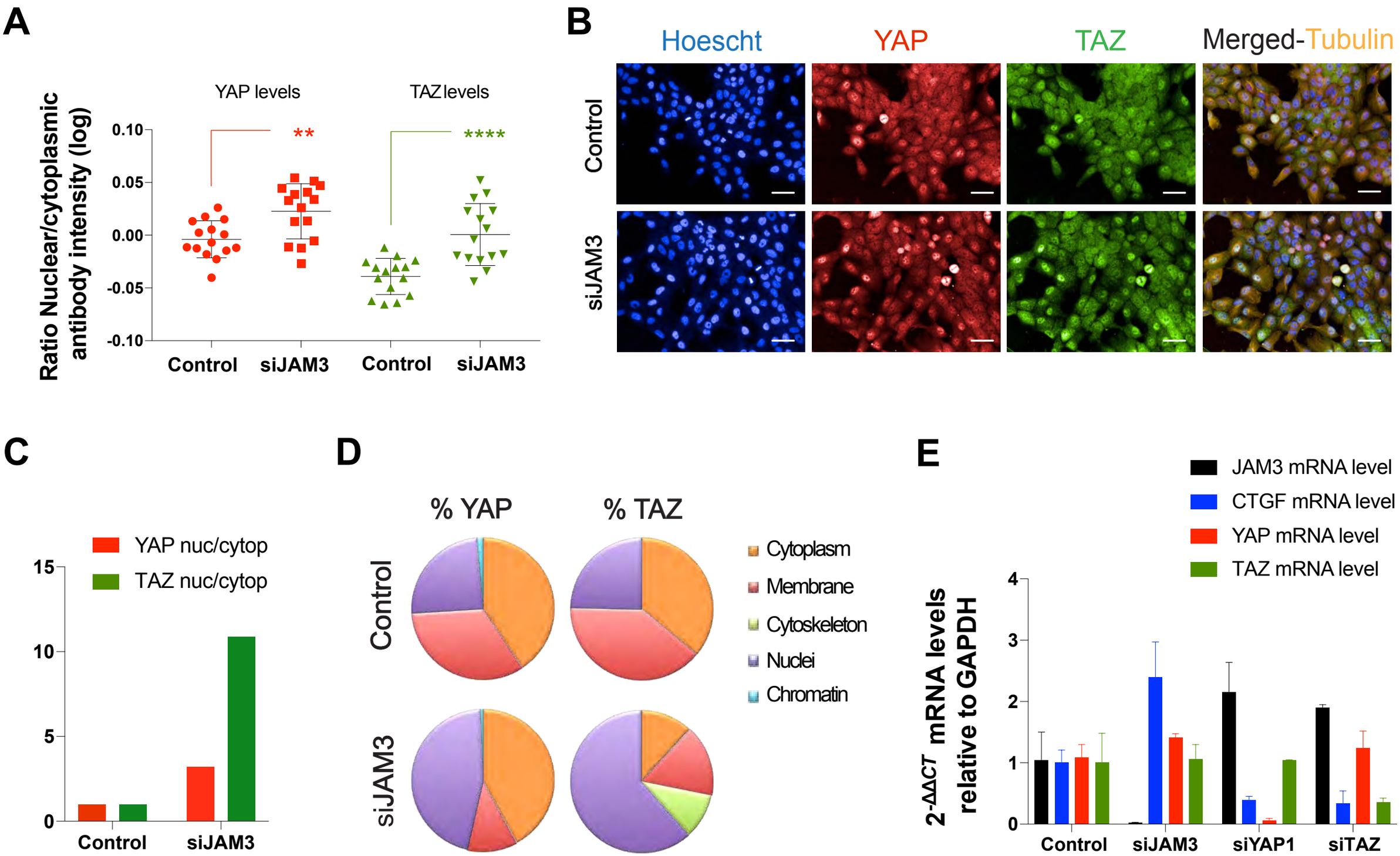

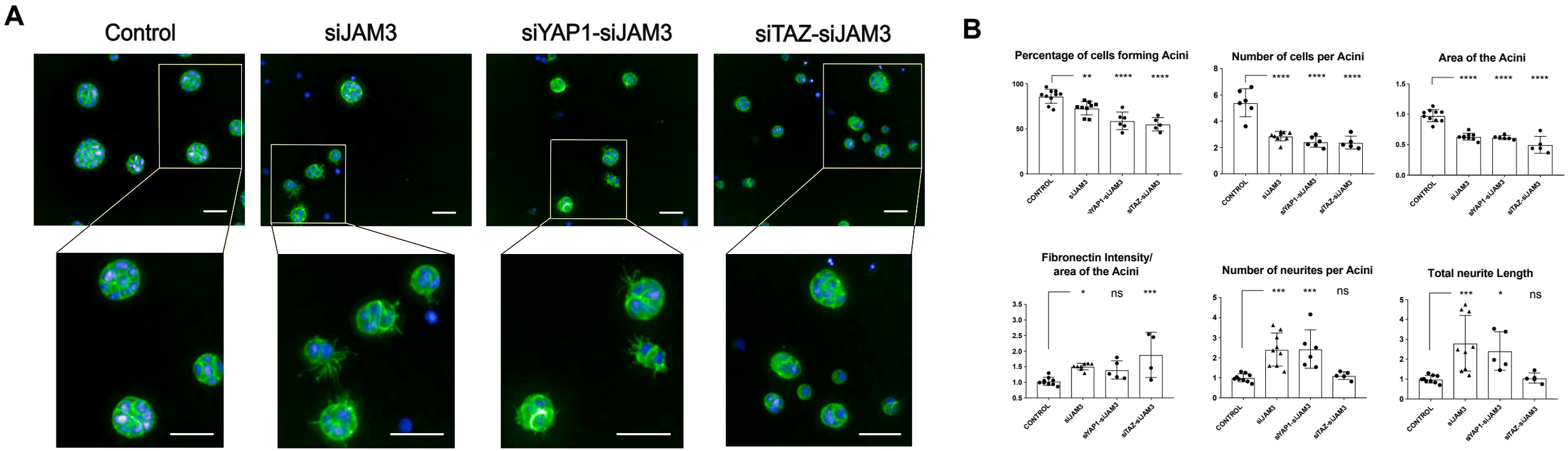

Figure 6. Arias-Garcia et al.

Figure 7. Arias-Garcia et al.

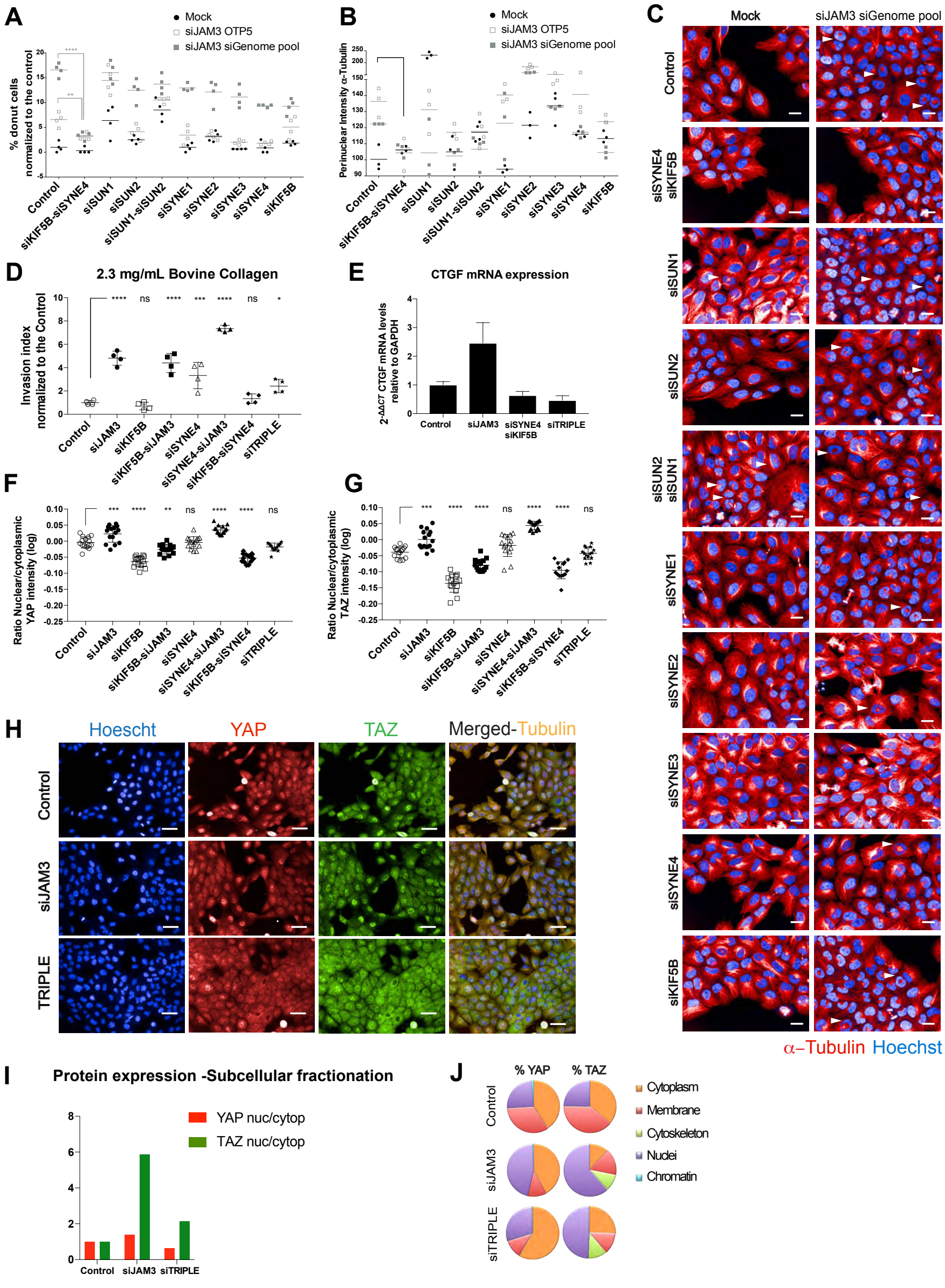

Figure 8. Arias-Garcia et al.

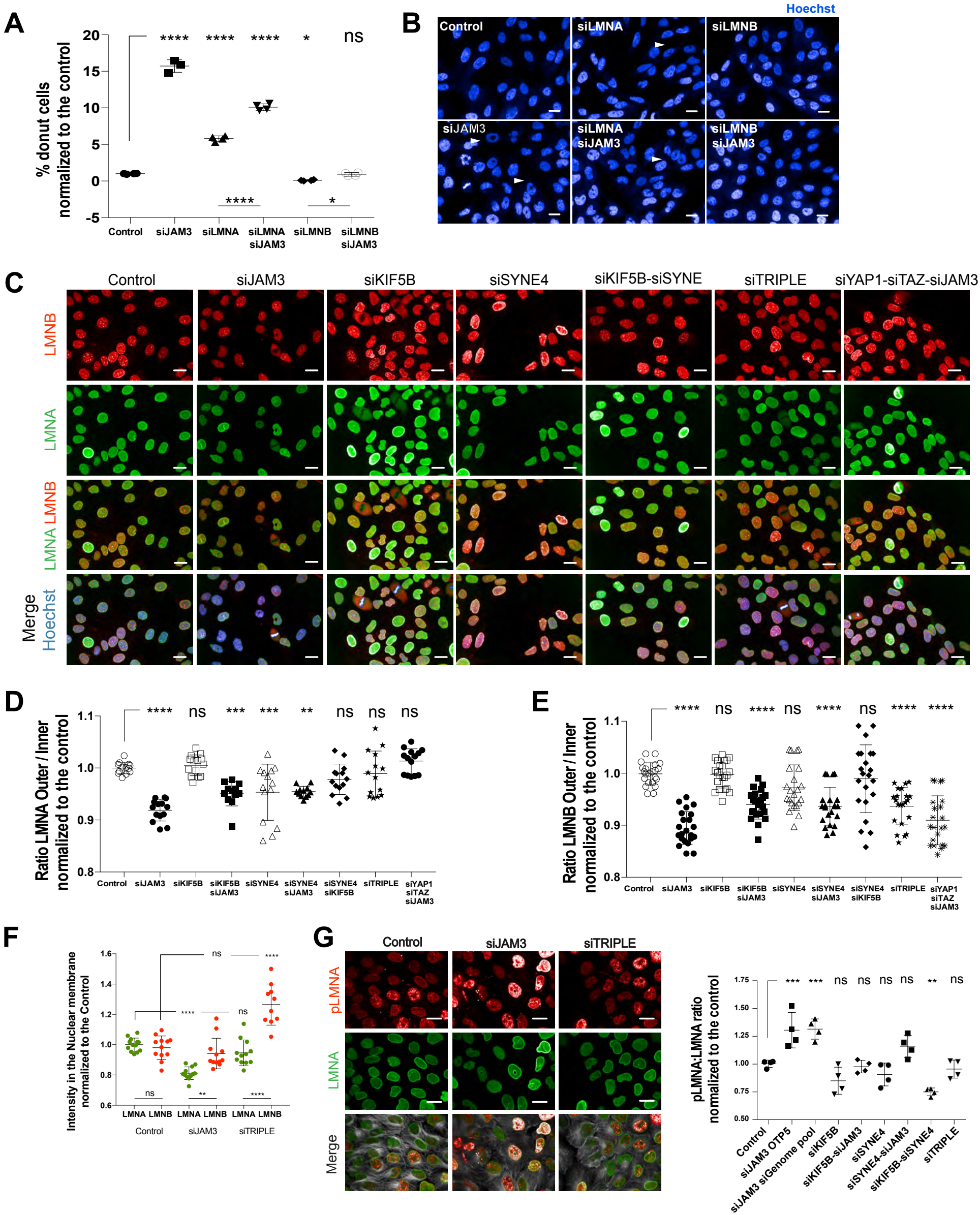

Figure 9. Arias-Garcia et al.

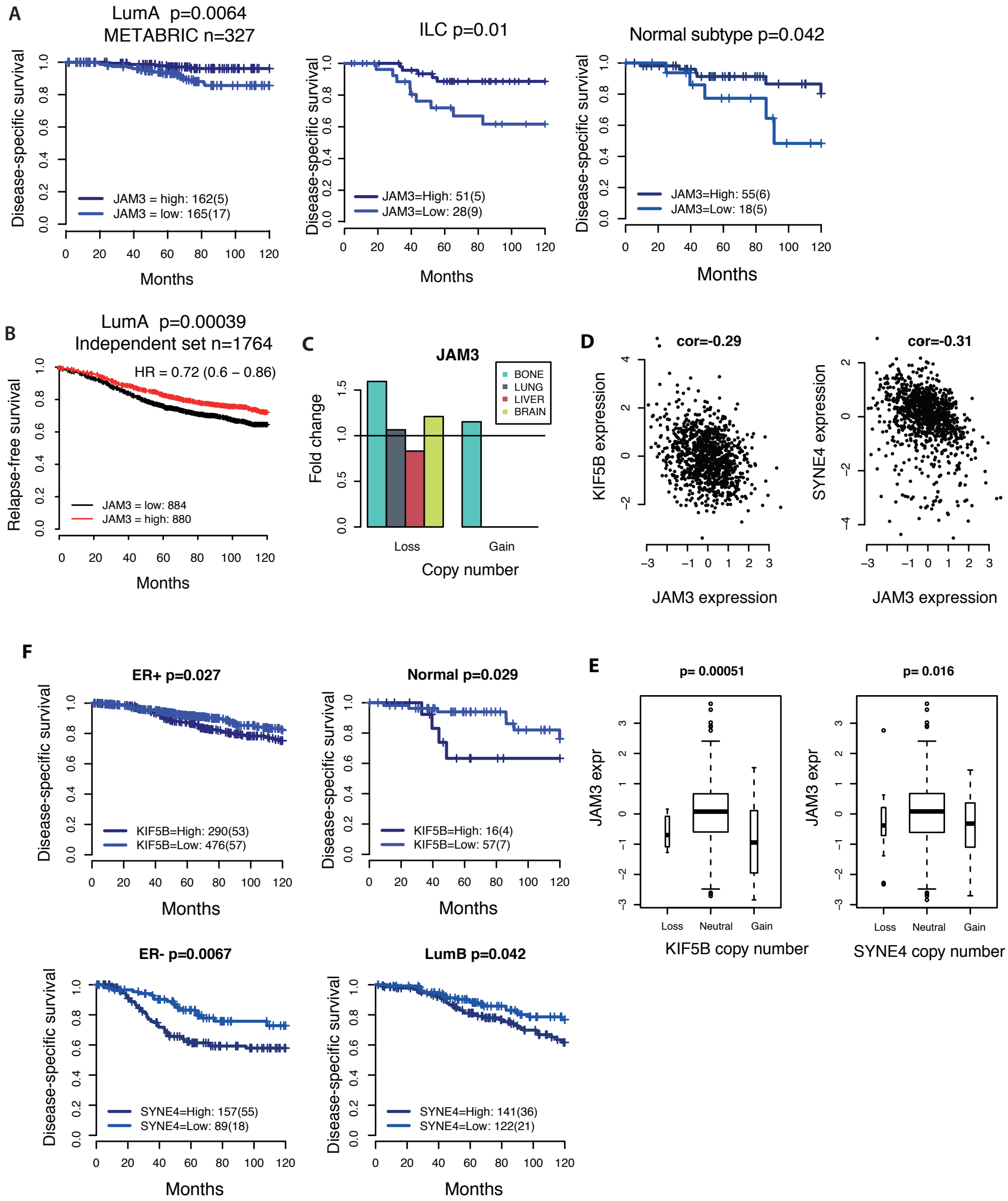
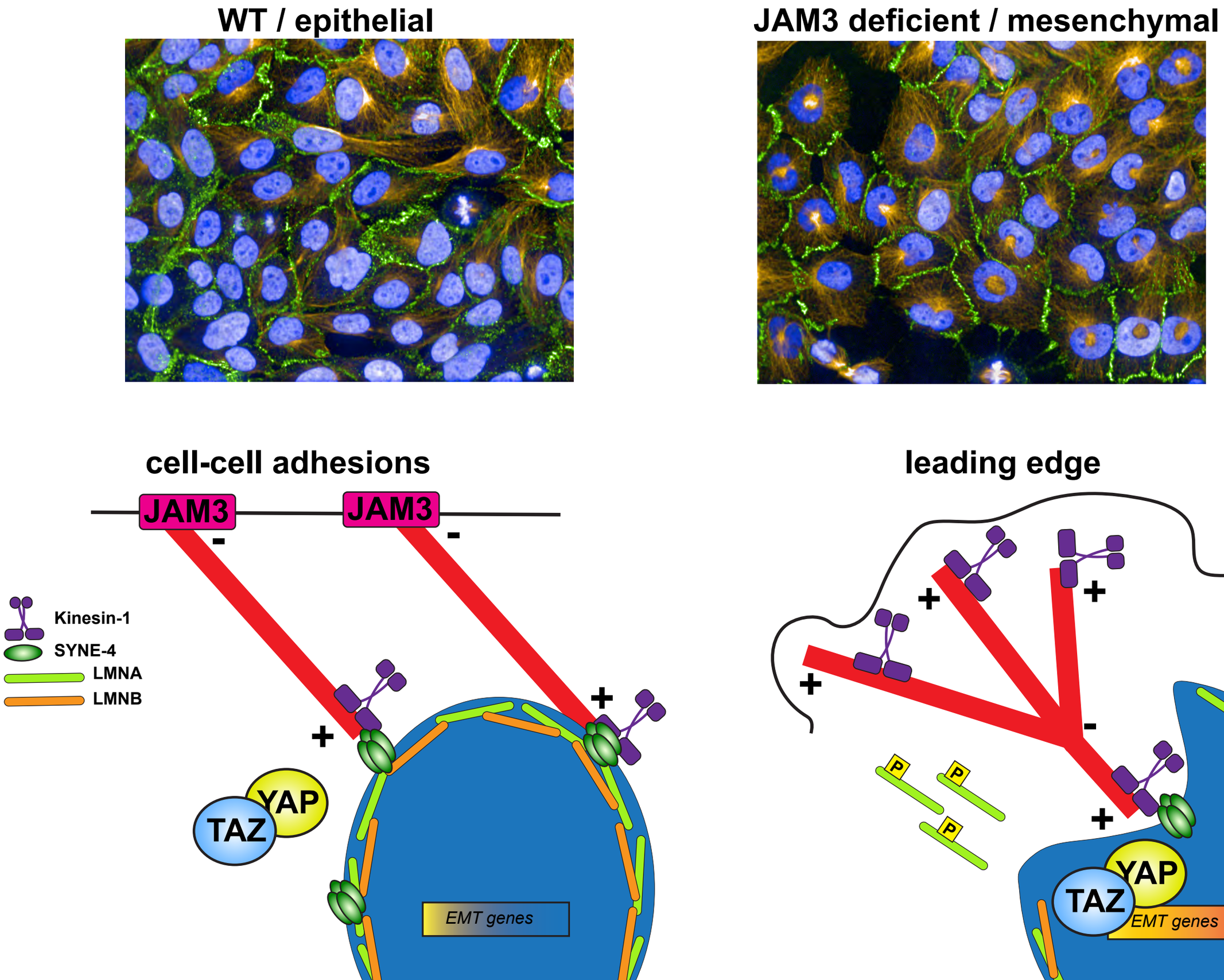
Figure 10. Arias-Garcia et al.